AD_____

Award Number:
W81XWH-11-1-0768

TITLE:
Refining an Automated Transcranial Doppler System for the Detection of Vasospasm after Traumatic Brain Injury

PRINCIPAL INVESTIGATOR:
Pierre D. Mourad, PhD

CONTRACTING ORGANIZATION:
University of Washington, Seattle WA 98105

REPORT DATE:
September 2014

TYPE OF REPORT:
annual report

PREPARED FOR: U.S. Army Medical Research and Materiel Command
Fort Detrick, Maryland 21702-5012

DISTRIBUTION STATEMENT:

☒ **X** Approved for public release; distribution unlimited

REPORT DOCUMENTATION PAGE

Form Approved
OMB No. 0704-0188

1. REPORT DATE	2. REPORT TYPE	3. DATES COVERED
September 2014	annual	1 Sep 2013 - 31 Aug 2014

4. TITLE AND SUBTITLE

Refining an Automated Transcranial Doppler System for the Detection of Vasospasm after Traumatic Brain Injury

5a. CONTRACT NUMBER

5b. GRANT NUMBER
W81XWH-11-1-0768

5c. PROGRAM ELEMENT NUMBER

6. AUTHOR(S)

Pierre D. Mourad, PhD

E-Mail: pierre@apl.washington.edu

5d. PROJECT NUMBER

5e. TASK NUMBER

5f. WORK UNIT NUMBER

7. PERFORMING ORGANIZATION NAME(S) AND ADDRESS(ES)

Applied Physics Laboratory, University of Washington, Box 355640
Seattle WA 98195-6470

8. PERFORMING ORGANIZATION REPORT NUMBER

9. SPONSORING / MONITORING AGENCY NAME(S) AND ADDRESS(ES)
U.S. Army Medical Research and Materiel Command
Fort Detrick, Maryland 21702-5012

10. SPONSOR/MONITOR'S ACRONYM(S)

11. SPONSOR/MONITOR'S REPORT NUMBER(S)

12. DISTRIBUTION / AVAILABILITY STATEMENT
Approved for Public Release; Distribution Unlimited

13. SUPPLEMENTARY NOTES

14. ABSTRACT

Traumatic brain injury (TBI) is a major contributor to morbidity and mortality experienced by those soldiers subjected to improvised explosive devices (IED) as well as in military and civilian high speed collisions. Traumatic cerebral vasospasm (TCV) is a major contributor to morbidity and mortality experienced by those TBI patients. Aggressive neurosurgical treatment motivated by early diagnosis appears to improve the clinical outcome for these patients. Early transcranial Doppler (TCD) measurements of blood flow speed within major cerebral arteries produces the initial diagnosis, hence motivates the rapid treatment of TCV. However, the skill necessary to deploy TCD limits its availability relative to its need. PhysioSonics, Inc, a local company in Seattle, created an *automatic* TCD system (called 'Presto' or aTCD) that minimizes the skill necessary to perform TCD assays. Our long-term goal is to optimize Presto for patients in vasospasm, through optimization of its spectral Doppler 'envelope' analyzer, its headset and supporting software so it can track blood flow in the internal carotid artery as well as middle cerebral artery.

15. SUBJECT TERMS
traumatic brain injury, ultrasound, transcranial Doppler, vasospasm.

16. SECURITY CLASSIFICATION OF:			17. LIMITATION OF ABSTRACT	18. NUMBER OF PAGES	19a. NAME OF RESPONSIBLE PERSON
a. REPORT	b. ABSTRACT	c. THIS PAGE			USAMRMC
U	U	U	UU	17	19b. TELEPHONE NUMBER *(include area code)*

Table of Contents

Page

INTRODUCTION – subject. Traumatic brain injury (TBI) is a major contributor to morbidity and mortality experienced by those soldiers subjected to improvised explosive devices (IED) as well as in military and civilian high speed collisions. Traumatic cerebral vasospasm (TCV) is a major contributor to morbidity and mortality experienced by those TBI patients. Aggressive neurosurgical treatment motivated by early diagnosis appears to improve the clinical outcome for these patients. Early transcranial Doppler (TCD) measurements of blood flow speed within major cerebral arteries produces the initial diagnosis, hence motivates the rapid treatment of TCV. However, the skill necessary to deploy TCD limits its availability relative to its need. This gap in patient care reduces the quality of care and potentially, therefore, the quality of life of injured soldiers. This gap also defines a critical need for robust, easy to use TCD system, applicable to these patients.

INTRODUCTION - purpose. Early work by the PI on automating transcranial Doppler has been translated by PhysioSonics, Inc, (PSI) a Seattle-based company that he co-founded into a working automated transcranial Doppler (aTCD) device called 'Presto' that they have submitted to the FDA via a 510K for approval. Their system is based upon a novel and proprietary ultrasound platform along with novel and proprietary 'search and lock on' algorithms for detecting and staying focused on the brightest spot in 'Doppler' space – that is, within ultrasound-derived maps of blood flow speed captured by their device. This is reasonable because a view of each of the major cerebral arteries relevant to vasospasm, listed below, shows that each contribute the largest values of blood flow, hence the largest signal in Doppler space. PhysioSonics has optimized it to measure blood flow speed within the middle cerebral artery (MCA) – sufficient for some assays of vasospasm, and demonstrated its utility on uninjured volunteers. However, a critical additional assay of vasospasm – the Lindegaard ratio - requires measurements of blood flow speed within the extra-cranial segment of the internal carotid artery as well as from the MCA. Moreover, while their system already works on humans, PhysioSonics has no plans to optimize the device for TCV, or to extract information from the ICA.

INTRODUCTION – scope of the research. To met the goal of this proposal we sought to test the following hypothesis: PhysioSonics' automatic TCD (aTCD) system, with modifications to its hardware and/or software as necessary, will match measurements of cerebral blood flow in the middle cerebral artery (MCA) and in the internal carotid artery (ICA) made by standard TCD on patients who suffer from cerebral vasospasm.

Specific Aim # 1: To test the ability of the aTCD device to measure blood flow velocity in the MCA and ICA of patients with known vasospasm, as compared to standard TCD run by a trained neurosonographer. *Proposed study:* Use the device to measure blood flow in the MCA and ICA of civilian vasospasm patients – typically those with sub-arachnoid hemorrhage – within Harborview Medical Center (HMC), the only Level One trauma center in Seattle. Compare those measurements with those determined during routine clinical care by the resident neurosonographer with their standard clinical TCD unit. Determine the level of fidelity of the aTCD-derived information on blood flow with that given by the gold standard, operator-dependent TCD device.

Specific Aim #2: To modify as necessary the TCD array and associated holder for use on the ICA, and, the algorithms required to extract the highest blood flow velocities in the MCA and ICA to guarantee that the aTCD device can detect the highest levels of vasospasm. *Proposed study #1:* Modify as necessary the brace that ordinarily holds the transducer to the temple (to facilitate measurement of blood-flow from within the MCA so that it will automatically extract blood flow information from the ICA. *Proposed study #2:* Modify as necessary the software within the aTCD device to optimize its ability to calculate the value of fastest blood flow within the MCA and the ICA for vasospasm patients. *Proposed study #3:* Modify as necessary the TCD transducer or its controlling software so as to optimize its ability to locate the point of fastest blood flow within the MCA and the ICA for vasospasm patients

Impact. Successful completion of the proposed work will yield a device that could readily become available to the military with its data interpreted on site or sent or via telemedicine for interpretation by distant neurosurgical experts.

BODY

Specific Aim #1: To test the ability of the aTCD device to measure blood flow velocity in the middle cerebral artery (MCA) and internal carotid artery (ICA) of patients with known vasospasm, as compared to standard TCD run by a trained neurosonographer. (Q1-Q10 out of 12 quarters)

Task 1: Get approval for the human subjects study (Q1-2). This study will involve up to 128 patients with vasospasm, with multiple studies per patient, over the three years of the study.

(1.1) **Done in the first year.**

Task 2: Take possession of the aTCD system (Q3).

(2.1) **Done in the first year.**

Task 3: Modify the software associated the aTCD system so it will report and store the spectrogram derived from each of the MCA and ICA, including the Lindegaard ratio. (Q2-5).

(3.1) **Done in the first year.**

Milestone #1: Achieve ability to start human study. **Done.**

Task 4: Modify as necessary the commercial headband that holds the TCD so that it can deploy on the upper portion of the neck of *volunteers*. (Q1-2)

(4.1) **Done in the first year.**

Task 5: Collect then archive aTCD and standard TCD data from the MCA and ICA of 128 patients, along with appropriate supporting medical data. For a subset of these patients we will also collect standard TCD data twice in a day in order to determine the length of time we will need to eventually monitor patients with our aTCD (Q3-Q10) UW.

(5.1) We started to recruit patients with civilian vasospasm in the 5/12th quarter of our study (October 2012). Table 1 documents the number of patients identified, consented, and studied during year two of this research effort (October 2012 – September 30th 2014).

Human Data	Identified	Consented	Studied	# of data sets
Total 1Oct2012-15Sept2013	**65**	**22**	**16**	**25**
1Oct2013 – 30Sept2014	**148**	**37**	**34**	**46**

Note that we loose two thirds of our identified patients to: lack of bone windows, lack of available next of kin, refusal to participate (a big problem because these patients are typically awake but uncomfortable), lack of cranial bone and patient death.

Task 6: Compare spectrogram features found within aTCD and standard TCD data. (Q5-Q10) UW

(6.1) In Figures 1-3 we compare representative blood-flow data in the MCA of three vasospasm patients. (Note that we get pdfs from the commercial system whose resolution for this report fall short of adequate representation when reproduced here.) These examples demonstrate that we can collect TCD data from the MCA of patients, with a mix of success in their comparison with the gold standard data, in ways that have or will produce improvements in the aTCD system.

Our system's data falls short in two key areas – the search algorithm and the spectral envelope calculation – as anticipated during the construction of this grant application. Indeed, our tasks as originally designed below seek to address these issues. As described in our 2nd annual report, we modified the aTCD device to search deeper, where our previous maximum depth was 50 mm and is now 70mm. We have now also added a feature where the user is able to force the machine to find peak flow in a certain volume of depth, by moving search box covering 10 mm vertical distance – this is described in detail in Task 10 below. This is meant to address some issues of the locking flow selection feature, where non-peak flow was selected.

Also, here we show the standard TCD system's reports of mean flow speeds, e.g. 107 cm/s at a depth in the left MCA of 50 mm, and pulsatility index (PI), a relative measure of the tendency of the peak systolic blood flow speed to rise above the mean blood flow speed. The aTCD system also reports these values, but in a different window. We will develop quantitative comparisons of these quantities as well as of peak systolic blood flow speed. Also, our ICA measurements with the aTCD system compare favorably with that of the clinical system. We have focused on those measurements that motivate changes to the aTCD system here for this report.

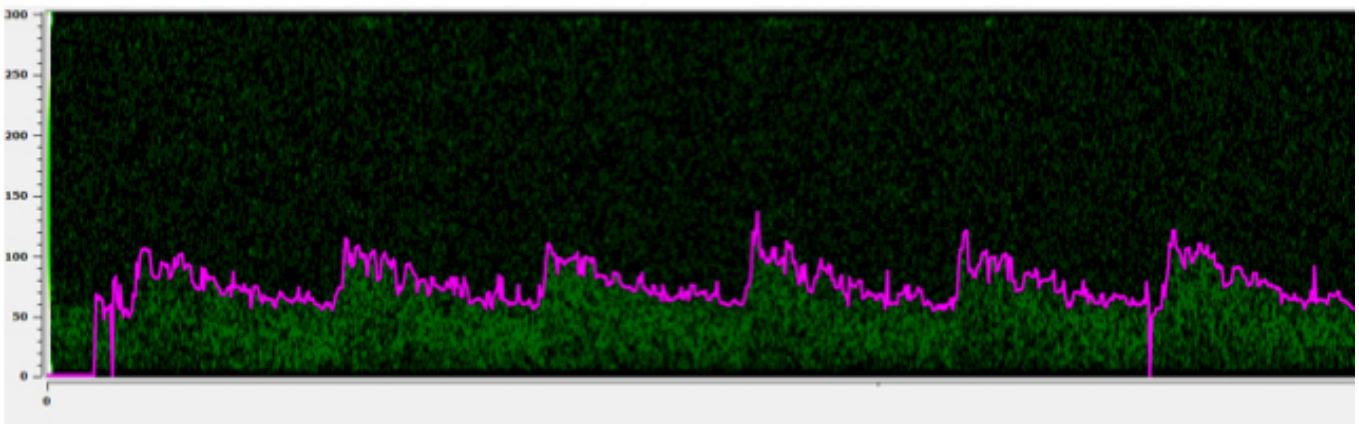

A

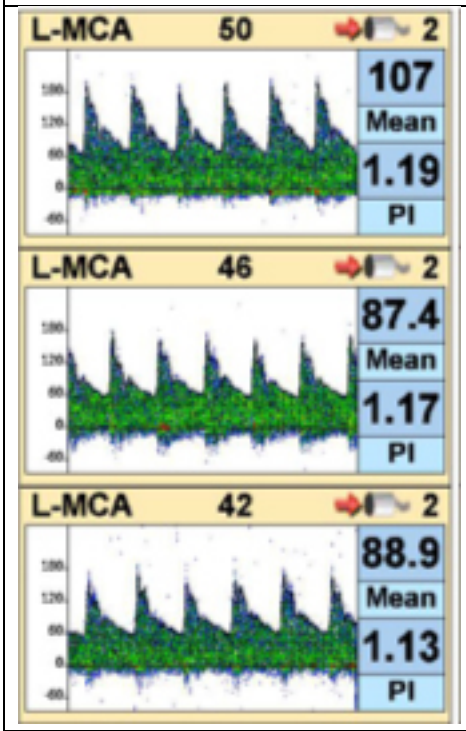

B

Figure 1. Data from the aTCD machine (A) and a standard TCD machine (B), where the aTCD data under-represents blood flow speeds in the MCA. Here in **(A)** we see peak systolic velocities identified by the commercial spectral envelope varying between 100-150 cm/s. However, in **(B)** the figures show that the standard TCD machine, with user intervention, measures peak systolic velocities as a function of distance from the transducer [at 50, 56 and 42 mm distance] with values closer to 180 cm/s. The aTCD machine provides data suggesting this patient is in mild vasospasm while the clinical machine demonstrates that this patient is in severe vasospasm. Therefore, for this patient, *the flow-envelope calculator fails to capture peak flow values.*

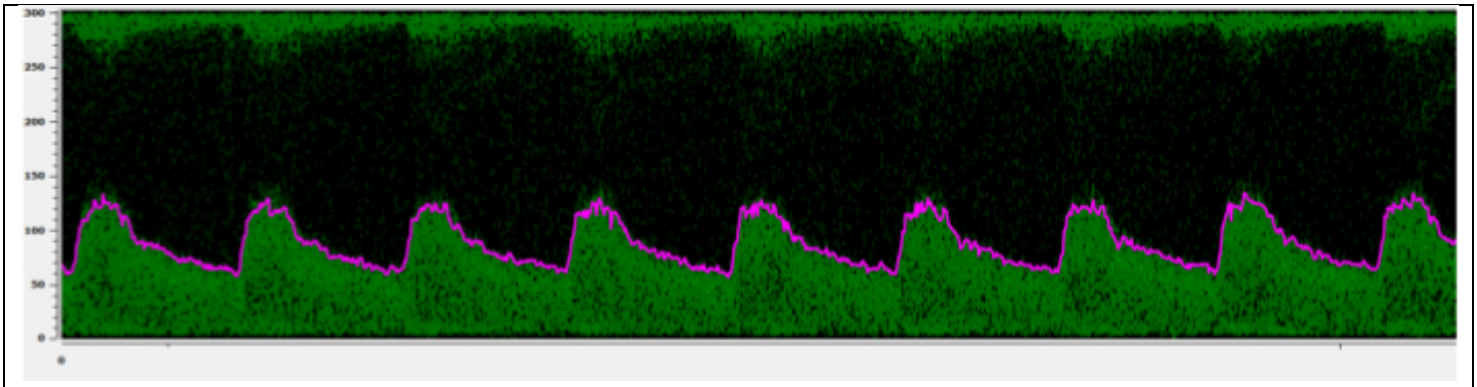

A

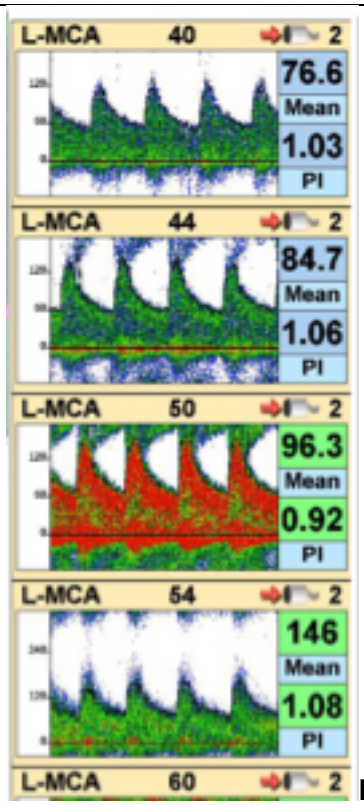

B

Figure 2. Data from the aTCD machine (A) and a standard TCD machine (B), where the aTCD data well represents the blood flow speeds in the MCA as defined by the standard TCD machine. Here in **(A)** we see peak systolic velocities identified by the commercial spectral envelope (in fucia) 140-150 cm/s, nominally close to the underlying spectrogram (in green). This compares favorably to measurements of peak systolic blood flow speeds **(B)** by the standard TCD machine as a function of depth [at 40, 44, 50 and 54 mm distance from the transducer]. These peak speeds start at a value of 120 cm/s at 40 mm distance from the transducer, increasing to close to 150 cm/s by 54 mm distance. Both the aTCD machine and clinical machine demonstrates that this patient is in moderate to severe vasospasm. Therefore, for this patient, *the aTCD system performs plausibly well compared to the clinical system.*

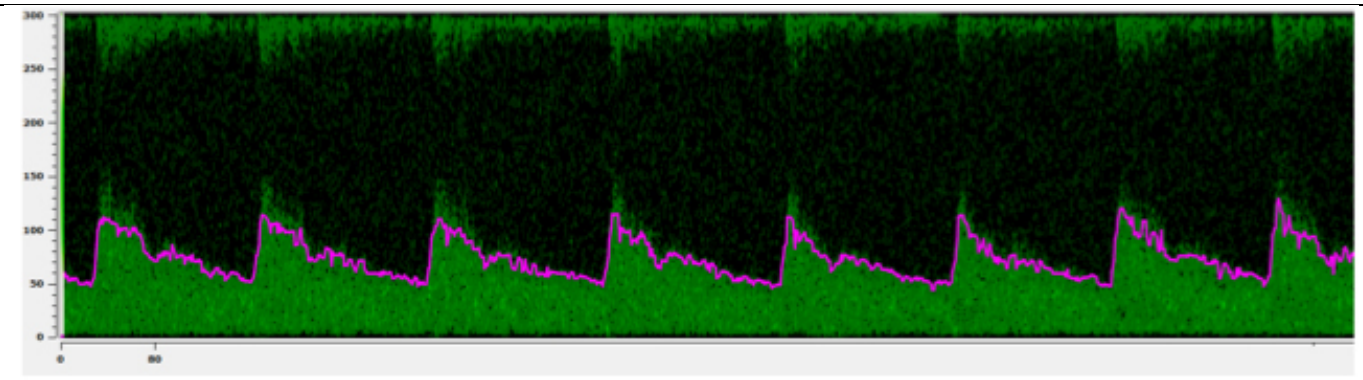

A

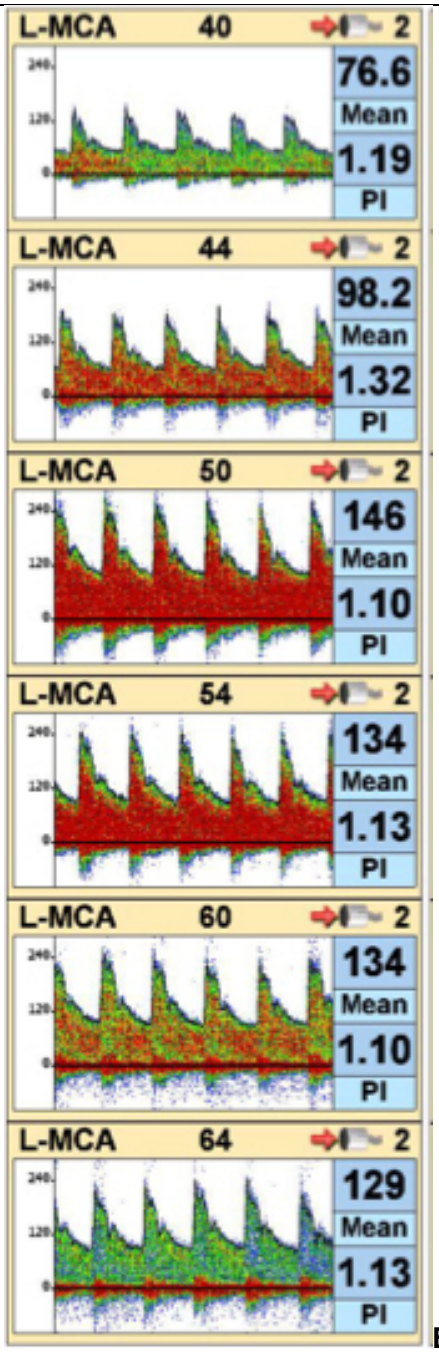

B

Figure 3. Data from the aTCD machine (A) and a standard TCD machine (B), where the aTCD data collects representative blood flow speeds in the MCA, but with a poor spectral envelope calculation, and at too shallow a depth, as compared to the data collected by the standard TCD machine. Here in **(A)** we see peak systolic velocities identified by the commercial spectral envelope (in fucia) 110 cm/s, woefully low compared to the 150 cm/s readily identify in the underlying spectrogram (in green). These 'green' values of blood flow speed compare favorably only to measurements of peak systolic blood flow speeds **(B)** by the standard TCD machine at its shallower depths (between 44 and 50 mm distance from the transducer face). The aTCD search algorithm completely misses the very high flow speeds captured by the standard TCD machine, namely, at or over 240 cm/s between depths of 50-64 mm. Therefore, for this patient, *the flow-envelope calculator fails to capture peak flow values and the device's search algorithm locks onto local peak flow velocities that are too shallow,* compared to the manually steered standard TCD system.

Milestone #2: Develop quantitative comparisons of the aTCD-derived and standard TCD-derived blood flow data from vasospasm patients, thereby highlighting short comings, if any, of the aTCD system for the case of vasospasm.

We have collected sufficient number of data sets from our patients to identify three problems with our existing aTCD system: [1a] the flow-envelope calculator fails to capture peak flow values and [1b] the device's search algorithm locks onto local peak flow velocities at too shallow a depth for many patients with vasospasm, all relative to the clinical gold standard. In addition, thanks to the formation of peripheral edema in several of these patients, we can say that [1c] the device's search volume is too shallow for an appreciable percentage of patients with vasospasm. Task 9 addresses problem #1a while Task 10 addresses problems #1b,c.

Task 7: Write up results for publication and presentations. (Q7-8; Q10-12) UW

(7.1) The Journal of Ultrasound in Medicine has published our paper (Marzban et al, 2013) that describes our first robust means of calculating optimal spectrogram envelopes for different patients. We have submitted two additional papers. One describes a second means of calculating optimal spectral envelopes, one based upon a first principles method described in our previous report with final results summarized in Figure 6, below. We have submitted a third paper associated with this project, one based upon a new statistics-based modeling effort for calculating spectra, which we report below (Marzban et al, 2014).

Milestone #3: get feedback on the quantitative aspects of our work from our scientific and clinical peers.

Our clinical peers are quite excited by the prospect of successful semi-automation of the TCD process but recognize that we've a ways to go before we succeed. In particular, our military TCD consultant, Alex Razumovsky, PhD, has verified the importance of this approach to TCD measurements and has asked us to (a) increase the depth of field of search for fastest blood flow, to (b) improve the signal-to-noise ratio of our system, to (c) explore use of an intermediate variable – a time-varying map of the MCA based upon creation of an 'iso-surface' of Doppler-derived blood-flow speeds – a 'Doppler map', discussed below – to map the blood-vessel structure sufficiently to visualize the MCA in vasospasm. This last issue is particularly important because some patients after blast show large blood flow speeds in the MCA not because they are in vasospasm but because their hematocrit is sufficiently low that the resulting reduced effective viscosity of the blood allows for higher than normal blood flow speeds.

We have one paper in print, and now have submitted two more papers that describe and exercise our flow envelope calculation.

Specific Aim #2: To modify as necessary the TCD holder for use on the ICA, and, the algorithms required to localize as well as extract the highest blood flow velocities in the MCA and ICA, in order to guarantee that the aTCD device can detect the highest levels of vasospasm. (Q3-Q12 out of 12 quarters)

Task 8: Modify as necessary the brace that ordinarily holds the transducer to the temple (to facilitate measurement of blood-flow from within the MCA) so that it will also automatically extract blood flow information from the ICA of *patients*. (Q4-Q8) PSI

(8.1) Our third version of the head set (reported in our second Annual Report) now covers both the MCA and internal carotid arteries. Patients remain uncomfortable using any headset, however. We are considering implementation of three-dimensional printing paradigms to produce an entirely new headset. We will perform this work at UW. Ivan Owen will likely participate in that effort. He is an expert in three-dimensional printing.

Milestone #4: Deliver device that holds the transducer that supports the measurement of blood flow velocity in the MCA and ipsilateral ICA for its deployment in Aim #1. ***Done.*** We've encountered an important practical problem for this study, however, namely that no test subjects wish to use the headset, given the general discomfort of our patients, all of whom have not had sufficient subarachnoid hemorrhage to require induction of a therapeutic coma. The headset is comfortable enough, as tested by engineers. The vasospasm patients are profoundly uncomfortable, however, and not obliged to wear the headset per our existing IRB protocol. We will talk to the program manager about adding a new Task to this study where we will refine the designs of this headset using feedback from healthy volunteers.

Task 9: Modify as necessary the software within the aTCD device to optimize its ability to calculate the

value of fastest blood flow (the spectral envelope) within the MCA and the ICA for vasospasm patients. (Q4-Q10) UW and PSI

First recall that the device as delivered will report values of the spectral envelope. Our job requires optimization of this process for vasospasm patients, a notoriously difficult cohort. We have identified two pathways towards development of optimized means of calculating the value of fastest blood flow in the MCA and ICA, referred to here as the spectral envelope: a statistical analysis and a mathematical modeling analysis. We have published results from the first pathway and continue to refine the details of the second method. We have now begun the process of initiating data collection on vasospasm patients at Swedish Medical Center here in Seattle using a certain standard TCD device that allows us to access the raw flow data. We have had difficulties recruiting enough patients that actually enter vasospasm, so this expansion will, hopefully, lead to a greater vasospasm sample size on which to test our enveloping algorithms. We hope to begin collecting data on vasospasm patients at Swedish by the end of 2014.

(9.1) As reported earlier we have applied our Double-Gaussian spectral flow envelope calculator (Marzban et al, 2013) to our new vasospasm patients with success thus far. We have completed work on another means of calculating the spectral envelope. This new approach uses the 'mixture' paradigm of Marzban et al, 2013, where a sum of functions adds together to describe the distribution of blood-flow speeds a given instant in time, from which the point of fastest blood flow is derived for that instant. The recently published work assumed that the instantaneous distribution of flow was best modeled by a Gaussian function. Here (Marzban et al, 2014) we relax that assumption, making use of two alternatives – a 'skewed' Gaussian function and an entirely non-Gaussian function (Figure 4, Figure 5). The skewed-Gaussian function has two additional parameters – the shape parameters for the signal and the background components. The non-Gaussian function uses a kernel method to estimate the flow velocity distribution. We found that, when it worked, the non-Gaussian function produced moderately superior envelopes than the skewed-Gaussian, however it did not work for all patients. We found that the skewed Gaussian function produced better envelopes than the regular Gaussian function for the majority of patients and comparable envelopes (i.e., no worse) in some patients. I am happy to report that this paper has just been accepted, subject to minor revisions.

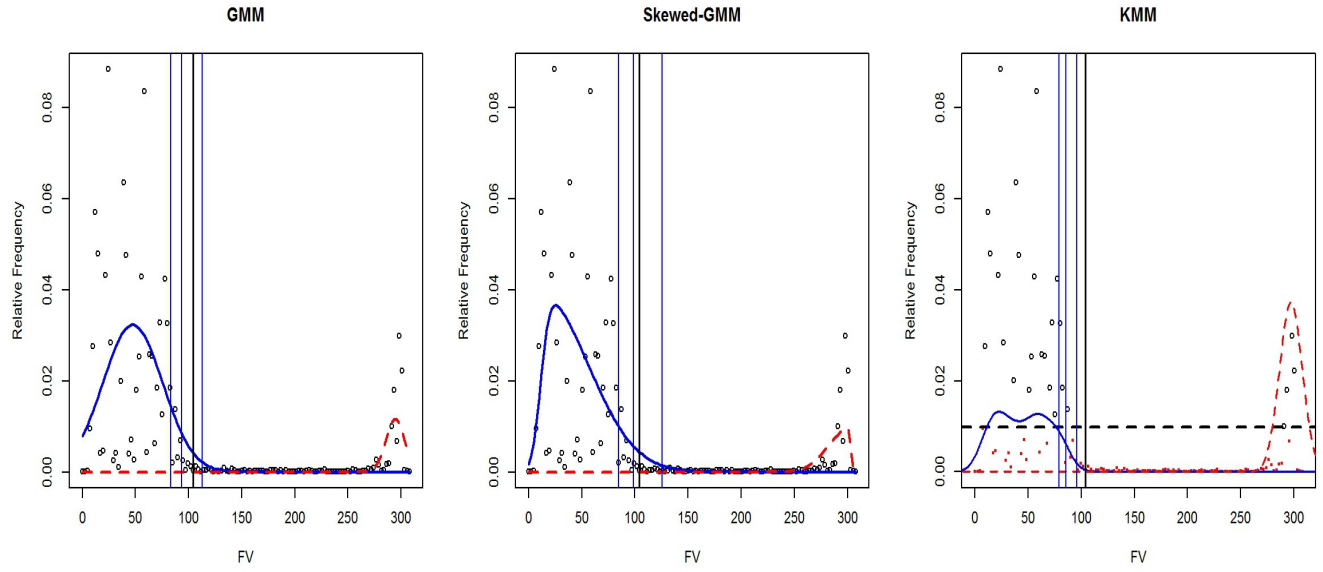

Figure 4. The distribution (more accurately, the probability density function) for the modeled signal (blue curve) and the background (red curve), as determined by mixture models – the Gaussian Mixture Model of Marzban et al, 2013 (GMM, left panel), Skewed-GMM (middle), and Kernel Mixture Model (KMM, right). The blue vertical lines denote the 90th; 95th; 99th percentiles of the signal flow velocity, and the black vertical line marks the maximum FV according to the industry standard Modified Geometric Method.

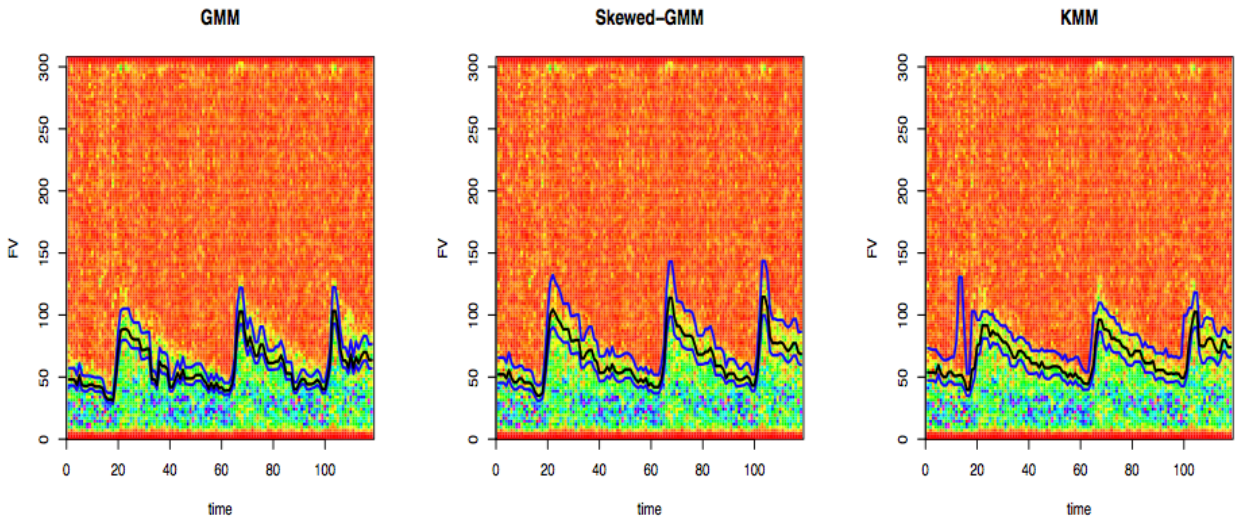

Figure 5. Sample spectrograms from our recently accepted paper (Marzaban et al. 2014), showing the fit of envelopes at the 90th, 95th, and 99th percentile of signal flow velocity for each of the Gaussian Mixture Model of (GMM, left), Skewed-GMM (middle), and Kernel Mixture Model (KMM, non-Gaussian, right).

We have submitted our paper on a second means of calculating optimal spectral envelopes, one based upon a first principles method described in our previous report with final results summarized in Figure 6, below.

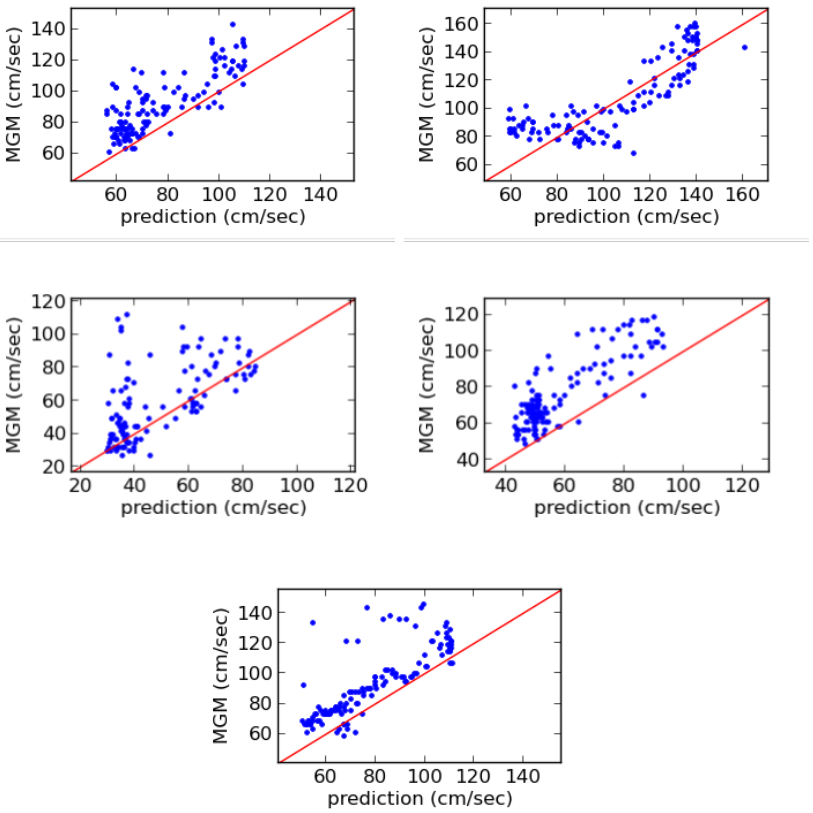

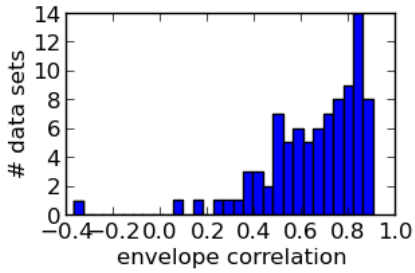

Figure 6 (left) Comparison of measured (horizontal axis) versus predicted (vertical axis) flow envelope for each of the five patients we studied in detail in Morison et al, (submitted). There is decent to good fit on average, with, however, a tendency of our model to over-predict the measurements. **(above)** Across many patients, the regression coefficient averages 0.7 with a full distribution noted above.

Milestone #5: Deliver software that robustly measures the values of fastest blood flow measured within the MCA and ICA for testing and validation in Aim #1. UW. As described above we have developed two plausible pathways to replace existing commercial algorithms for *calculating* the fastest blood flow with new ones optimized for vasospasm, where the signal to noise ratio is low and the blood flow speeds are high, each testing the limits of the existing system. In future work we will seek additional means of calculating this quantity as well as test these new methods on our existing data sets.

Task 10: *Modify as necessary the TCD's controlling software so as to optimize its ability to search for and locate the point of fastest blood flow within the MCA and ICA for vasospasm patients.* (Q4-Q10) UW; PSI

(10.1) In year 2, we achieved a first iteration of this Task. Our studies with patients made clear the need to have the 'search algorithm' look for points of fastest blood flow deeper than the standard 60 mm within each of the middle cerebral artery and the ICA. We have made that change (Figure 7, reported earlier) and reduced the noise in the collected data.

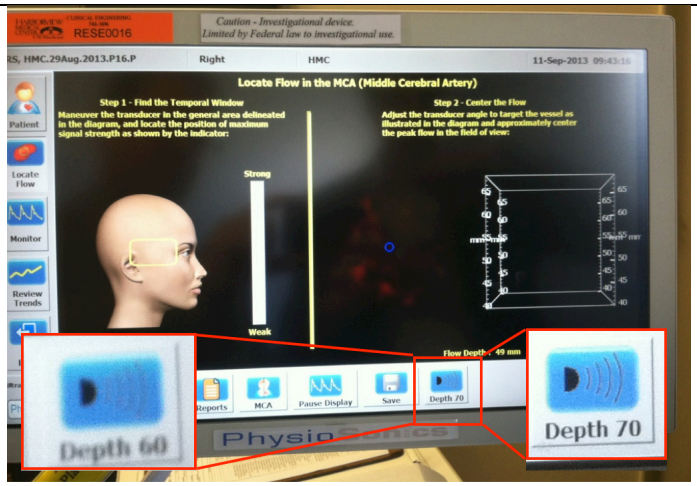

Figure 7. This figure shows the modified user interface that guides the user to setup the automatic TCD to locate the point of fastest blood flow in the middle cerebral artery. Here we photo-document (with a smart-phone camera) that the device can search up to 70 mm deep within the cranium. The user specifies the search depth (60 or 70 mm) and then lets the machine collect its data.

Despite the fact that our algorithm can search over a depth range up to 70 mm within the cranium, our search and locate algorithm thus far tends to lock on to plausible blood-flow maxima within the MCA at shallower depths (40-50 mm) as compared to the depth of vasospasm identified by the commercial TCD (50-65 mm), which facilitates search by hand for the global maximum in blood flow speed along the MCA. In Q9 we identified a potential solution to this issue and worked with our consultant Tom Anderson of Glacier River in Q10 to develop the necessary software changes. In Q11 we updated the search algorithm to allow the user to specify a search volume. Here, we have added a slider bar on the far right of the "Locate Flow" window that allows the user to slide a search box spanning 10 mm depth across the accessible volume (below, Figure 8a,b). We can access volumes between 40 mm and 70 mm. The search volume box can be moved in increments of 1mm. We can move the search volume box for both the MCA and ICA transducers. We continue to advance another portion of the search algorithm design to improve its means of identifying the point of fastest blood flow within a given volume.

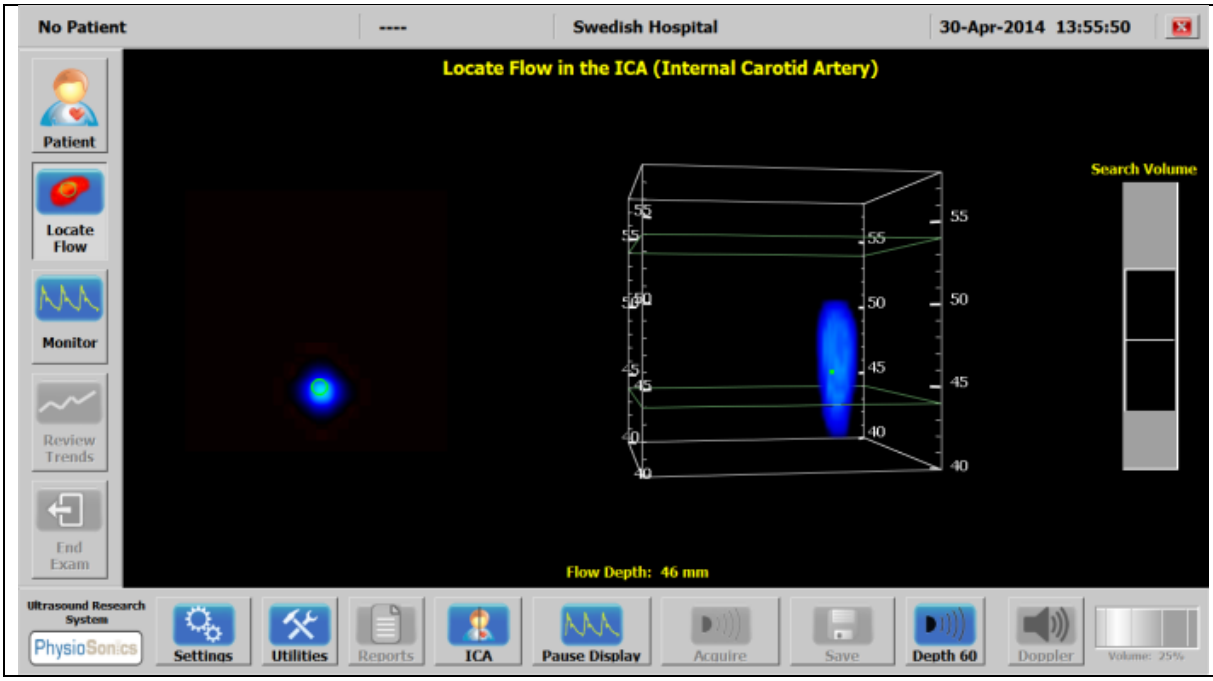

Figure 8a. Screenshot of the slider (far right) and search volume box (center, green lines bound the search box) when locating flow in the ICA.

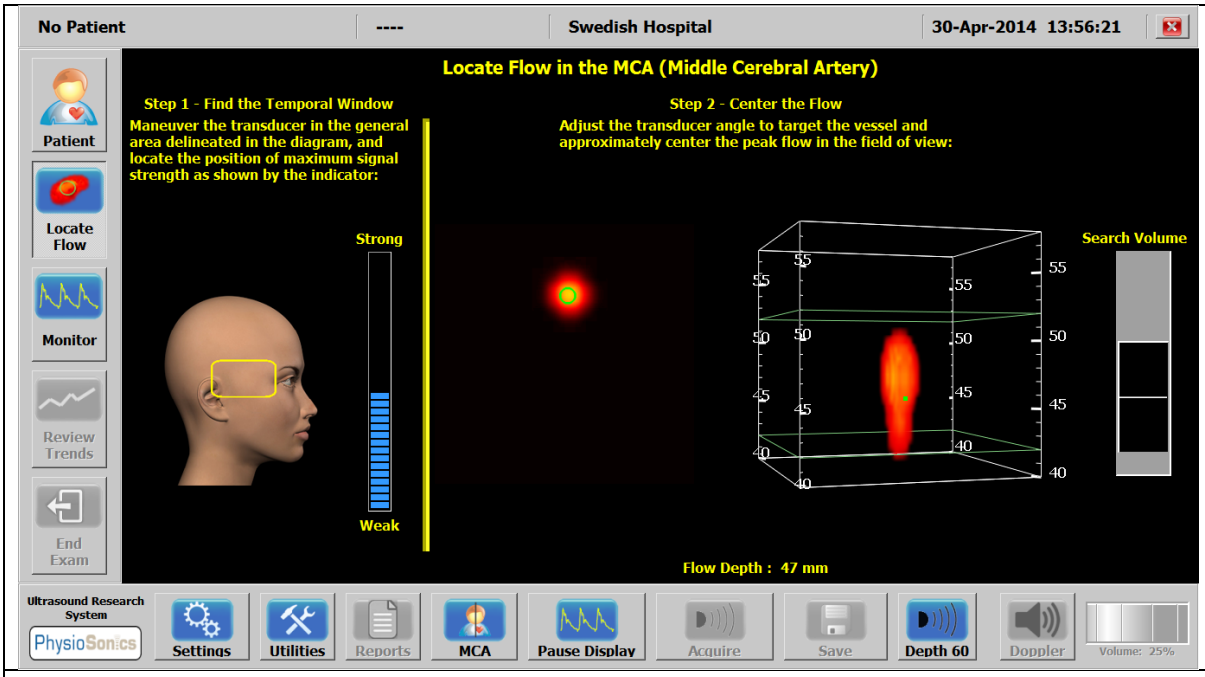

Figure 8b. Screenshot of the slider (far right) and search volume box (center, green lines bound the search box) when locating flow in the MCA.

(10.2) We started to determine what it will take to access an internal variable within the aTCD system that facilitates identification of the point of fastest blood flow within the cranium in the region of the MCA, by producing a time-varying map of an iso-surface of Doppler-derived blood-flow speed (Figure 9). The potential benefits the projects are three-fold. (1) We expect to refine the process of identification of fastest blood flow by analyzing how this system collects and processes this internal imaging data. (2) We expect to produce the ability to *visualize* vasospasm by directly measuring the diameter of the blood vessels through analysis of these Doppler maps. (3) Production of these maps may allow assessment of vasospasm in the case of low hematocrit (which can produce large values of blood flow speed without vasospasm0 by superimposition of the identified point of fastest blood flow with the associated vascular anatomy.

This will require substantial work 'under the hood' to make these data readily available for both off-line and real-time analysis. We have started the process of setting these internal tasks.

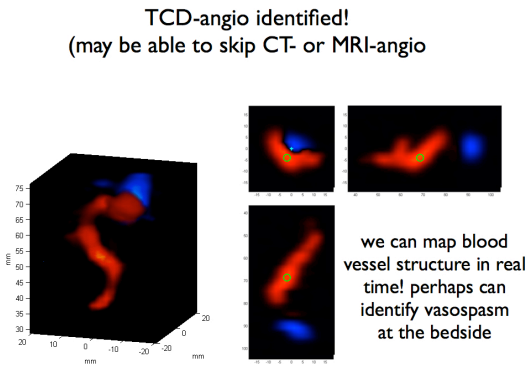

Figure 9. Samples of instantaneous three-dimensional maps of blood flow in the cranium. Here we display in one map a three-dimensional view of the internal carotid artery (in red) and where it meets the middle cerebral artery (MCA, in blue). Each color displays a single, absolute value of blood flow speed towards or away from the transducer, thereby outlining the blood vessel. The other three images offer three different perspectives on the MCA (in red) and the anterior communicating artery (blue), as well as locating the position of the point of fastest blood flow towards the transducer (green dot).

Milestone #6: Deliver software that optimally identifies the point of fastest blood flow in the MCA and ICA for vasospasm patients for testing and validation for its analysis in Aim #1. UW

Task 11: *Perform pilot study involving 32 patients that tests in a blinded fashion the efficacy of the aTCD compared with a standard TCD system.* (Q10-Q12). UW

(1) NA

Task 12: *Travel to a military medical facility under the sponsorship of Dr. Armonda to determine what changes, if any need to be made to the FDA approved aTCD system for optimal deployment to military facilities.* Q10-12). UW

(1) NA

Task 13: *Write up results in a final report for the sponsor, for publication, and within a follow-on proposal that will field trial an aTCD device at a military hospital involving patients with blast-induced TCV. (Q10-Q12). UW*

(1) NA

Milestone #7: Report results to the sponsor and begin the transition of this technology to the military.

KEY RESEARCH ACCOMPLISHMENTS

- We have created an improved headset for use in deploying simultaneous MCA and ICA monitoring.
- We have verified the existence of three technical obstacles between the current system and one useful for vasospasm detection and monitoring, all anticipated, as a class, in writing the original proposal. [1a] the flow-envelope calculator can fail to capture peak blood-flow values; [1b] the device's search algorithm locks onto local peak flow velocities at too shallow a depth for many patients with vasospasm; [1c] the device's search volume is too shallow for an appreciable percentage of patients with vasospasm.
- To address problem [1a] we have demonstrated several methods for calculating spectral envelopes, based on a Double-Gaussian function, a mixture paradigm, a skewed-Gaussian function, and an entirely non-Gaussian function. Of these, the initial Double-Gaussian function produced reasonable results and of the latter three, the skewed-Gaussian function performed best, producing better envelops than the regular Gaussian function for most patients, and comparable envelopes in some patients.
- Also to address problem [1a] we have demonstrated a potentially useful means of calculating spectral envelopes based upon local mathematical information, processed in a statistical way.
- To address problem [1b] we have added a function to the aTCD device, which allows the user to select a window of 10 mm width in which the machine should search for the peak flow. In this way, the user can force the machine to select the true point of peak flow (at a deeper point) than the false shallow point it often selects.
- To address [1c] we have, in year 2, modified the internal aTCD software in order to increase the depth over which the internal search algorithm will seek to identify the point of fastest blood flow in the MCA and ICA. We have verified that this modification works while in use on patients.
- In total, we have collected 71 data sets on 50 patients over the 2 years of patient data collection. We believe these low numbers occur due to a paucity of patients to consent relative to historical averages, and because only one third of the available patients are willing to participate due to their extreme discomfort. To address this problem we have identified a parallel site within the Seattle area (Swedish Hospital that appears willing to pursue data collection) and have initiated the IRB review process to collect data on a wider field of patients at Swedish.
- Also, at times the aTCD system requires upgrades that take it out of commission. To continue to collect data we have modified our IRB (with approval now from the local, UW committee) to continue to collect data with a modified standard TCD system, which will allow us to continue to accrue data in support of improving the spectral envelope.

CONCLUSIONS

- We can collect high quality TCD data using the aTCD system from vasospasm patients.
- In doing so we have, however, verified the existence of three technical obstacles between the current system and one useful for vasospasm detection and monitoring, all anticipated, as a class, in writing the original proposal. [1a] The flow-envelope calculator can fail to capture peak blood-flow values; [1b] the device's search algorithm locks onto local peak flow velocities at too shallow a depth for many patients with vasospasm; [1c] the device's search volume is too shallow for an appreciable percentage of patients with vasospasm.
- We have developed and implemented solutions to all three of these technical problems, which we continue to improve.
- We have also identified another problem, namely a reduced number of patients available for study, due to unusually good weather in Seattle [civilian subarachnoid hemorrhage often occurs in Seattle during times of bad weather] as well as a reluctance of these patients to participate in the exam because they are awake but extremely uncomfortable, and use of the aTCD (versus a standard TCD system) is optional from a clinical perspective. To address this problem we have identified a parallel site within the Seattle area (Swedish Hospital that appears willing to pursue data collection) and have initiated the IRB review process to collect data on a wider field of patients at Swedish.

REPORTABLE OUTCOMES AND REFERENCES

(copies of these documents are attached to the end of this report, in the Appendix)

Marzban C, Illian PR, Morison D, Mourad PD (2013) A Double-Gaussian, Percentile-Based Method for Estimating Maximum Blood Flow Velocity. *J Ultrasound Med*. 32:1913–1920.

Morison D, Marzban C, Mourad PD (2013) A Model of Blood Flow based on Transcranial Doppler Ultrasound. Under construction.

Marzban C, Gu W, Mourad PD (2014) A Noninvasive Estimator of Intracranial Pressure. *Submitted to J Ultrasound Med.*

Marzban C, Gu W, Mourad PD (2014) Mixture Models for Estimating Maximum Blood Flow Velocity. *Submitted to J Ultrasound Med.*

A Double-Gaussian, Percentile-Based Method for Estimating Maximum Blood Flow Velocity

Caren Marzban, PhD, Paul R. Illian, BS, David Morison, BS, Pierre D. Mourad, PhD

Objectives—Transcranial Doppler sonography allows for the estimation of blood flow velocity, whose maximum value, especially at systole, is often of clinical interest. Given that observed values of flow velocity are subject to noise, a useful notion of "maximum" requires a criterion for separating the signal from the noise. All commonly used criteria produce a point estimate (ie, a single value) of maximum flow velocity at any time and therefore convey no information on the distribution or uncertainty of flow velocity. This limitation has clinical consequences especially for patients in vasospasm, whose largest flow velocities can be difficult to measure. Therefore, a method for estimating flow velocity and its uncertainty is desirable.

Methods—A gaussian mixture model is used to separate the noise from the signal distribution. The time series of a given percentile of the latter, then, provides a flow velocity envelope. This means of estimating the flow velocity envelope naturally allows for displaying several percentiles (eg, 95th and 99th), thereby conveying uncertainty in the highest flow velocity.

Results—Such envelopes were computed for 59 patients and were shown to provide reasonable and useful estimates of the largest flow velocities compared to a standard algorithm. Moreover, we found that the commonly used envelope was generally consistent with the 90th percentile of the signal distribution derived via the gaussian mixture model.

Conclusions—Separating the observed distribution of flow velocity into a noise component and a signal component, using a double-gaussian mixture model, allows for the percentiles of the latter to provide meaningful measures of the largest flow velocities and their uncertainty.

Key Words—blood flow; brain; head injury; noninvasive; transcranial Doppler sonography

Received February 20, 2013, from the Applied Physics Laboratory (C.M., P.R.I., D.M., P.D.M.) and Departments of Statistics (C.M.), Neurological Surgery (P.D.M.), and Bioengineering (P.D.M.), University of Washington, Seattle, Washington USA. Revision requested March 6, 2013. Revised manuscript accepted for publication April 15, 2013.

This work was supported by National Institutes of Health grant R43NS46824-01A1, National Space Biomedical Research Institute grant SMS00701-2009-513, and PhysioSonics, Inc (Bellevue, WA). Dr Mourad has a financial interest in PhysioSonics.

Address correspondence to Caren Marzban, PhD, Department of Statistics, University of Washington, Box 354322, Seattle, WA 98195-4322 USA.

E-mail: marzban@stat.washington.edu

doi:10.7863/ultra.32.11.1913

Transcranially derived Doppler measurements of blood flow in major cerebral arteries have found many clinical applications.[1] In addition to assaying stroke risk due to sickle cell disease, dysfunction of cerebral autoregulation, and a patent foramen ovale, among other etiologies, some of the earliest applications targeted monitoring for vasospasm after subarachnoid hemorrhage.[2–5] Cerebral vasospasm, the transient reduction of the diameter of 1 or more major cerebral arteries, can lead to reduced blood flow into the brain and hence cerebral ischemia and an increasing chance for neurologic damage.[1] Monitoring for the onset of vasospasm remains an important application of transcranial Doppler sonography, with more 30,000 patients per year requiring daily monitoring for 1 week or more.[6] Adding to this primarily

Author: Nonstandard abbreviations are written out, per journal style.

civilian population are military patients with head injuries after exposure to explosions, typically roadside bombs, with half of these patients having cerebral vasospasm.[7]

Transcranial Doppler sonography measures the distribution of blood flow speeds within a blood vessel toward or away from the transducer, with negligible flow speeds adjacent to the blood vessel wall and maximum flow speeds near the center of the vessel.[8] Critical for the assay of cerebral vasospasm, among other uses of **transcranial Doppler** sonography, is successful capture of the speed of the fastest flowing blood within the major cerebral arteries, since this value acts as a useful proxy for blood vessel narrowing.[1] Capturing this speed is a particularly challenging problem, since vasospasm reduces the volume of blood flow while accelerating the blood flow speed,[9] hence reducing the target for transcranial Doppler measurements while straining against the upper limits of ultrasound data processing due to aliasing.[10]

The time series of a flow velocity histogram is generally referred to as a spectrogram, and the time series of the maximum flow velocity is called an envelope. Although the spectrogram conveys a great deal of information, the envelope is often the only quantity a clinician examines. This practice is reasonable because the information contained in a spectrogram can be displayed in different ways, leading to different conclusions. For example, Figure 1 shows a spectrogram with 2 different color schemes; in the top panel, the spectrogram is linearly related to the color scale, whereas in the bottom panel, the colors are proportional to the square root of the spectrogram.

Figure 1. Spectrograms of 2 different mappings for assigning color to the flow velocity (FV) values: linear (top) and square root (bottom).

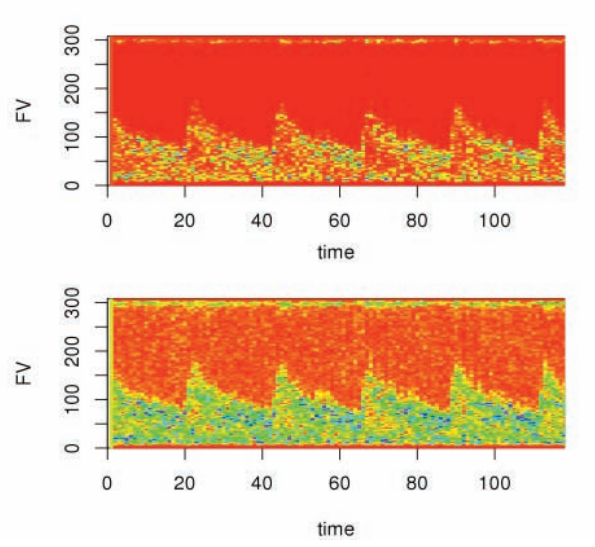

This inherent ambiguity in the information gleaned from a spectrogram also reflects itself in the corresponding envelope. In practice, observed flow velocity values can range from 1 to 300 cm/s. Therefore, to obtain a useful estimate of maximum flow velocity, one must introduce some criterion that defines what is meant by maximum. Many such criteria (standards for transcranial Doppler measurements[11–15]) are based on the cumulative histogram of flow velocity. Figure 2 shows an example of the relative frequency histogram of flow velocity (top) and the corresponding cumulative histogram (bottom) at a specific time for a specific patient (hereafter, patient X); the latter is obtained by integrating the former from left to right. One may define the maximum flow velocity as the value at which the cumulative histogram "levels off," but there exist different criteria corresponding to different objective measures of that point.[11–15] The vertical bar in Figure 2 marks the flow velocity at which it is maximum according to the modified geometric method.[11,12] The top panel in Figure 3 shows the spectrogram and the modified geometric method envelope (in black) for patient X.

Given that the proposed algorithm is compared with the modified geometric method algorithm, a brief review of the latter is in order. The modified geometric method algorithm and its variants[11,12] effectively rotate (clockwise and about the origin) the cumulative histogram by some amount. The effect of such a rotation is that the point at which the cumulative histogram levels off translates to a point at which the rotated cumulative histogram reaches

Figure 2. Histograms of flow velocity (FV) for patient X at a given instant in time (top), and the corresponding cumulative (ie, integrated) histogram (bottom).

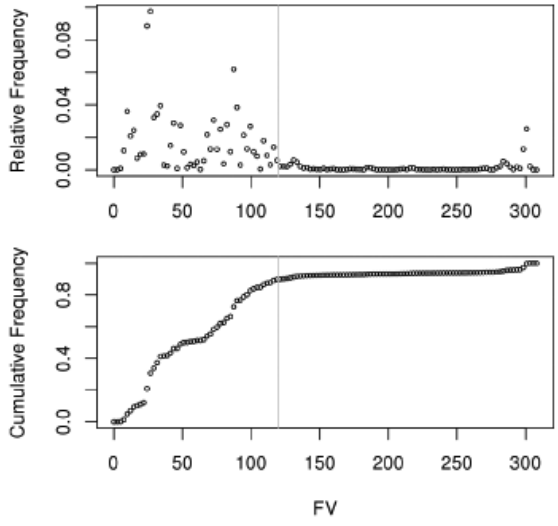

the maximum. Given certain smoothness constraints, it has been shown that this point corresponds to the maximum flow velocity.[12] Note that the modified geometric method algorithm generates only point estimates of the maximum flow velocity and so provides no natural measure of uncertainty. This limitation is evident in the cumulative histogram in Figure 2: Although the modified geometric method provides an estimate of the point at which the cumulative histogram levels off, quantifying the corresponding uncertainty is by no means unambiguous. Conveying uncertainty is important because different levels of uncertainty call for different clinical actions.

The main proposals in this study were (1) to develop a new means of separating the noise and the signal components of a spectrogram and (2) to quantify the largest values in the signal using the concept of percentile. The *n*th percentile of a quantity x is defined as the value of x for which n% of the x values are smaller. For example, the 95th percentile of flow velocity is the flow velocity value at which 95% of flow velocity values are smaller. An envelope based on the 95th percentile of the histogram, then, provides a meaningful estimate of the "top 5%" of flow velocities. Moreover, 2 (or more) envelopes at different percentiles can convey some notion of uncertainty. In this study, envelopes based on 3 percentiles were considered: 90th, 95th, and 99th.

Figure 3. Top, Spectrogram for patient X (color background) and 4 estimates of the envelope: modified geometric method envelope (black) and 90th, 95th, and 99th percentile-based envelopes. Bottom, Modified geometric method envelope (black), 95th percentile-based envelope (red), and 90th and 99th percentile-based envelopes (blue). FV indicates flow velocity.

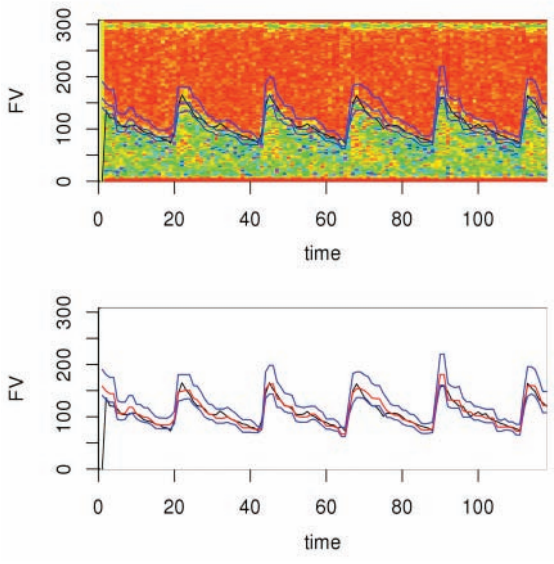

The use of a percentile to quantify the largest flow velocity presumes that the histogram is the correct histogram of flow velocity. In practice, observed spectrograms are contaminated by various types of noise. One of these sources of noise is evident in the small "hump" appearing on the right side of the (relative frequency) histogram in Figure 2. Flow velocity values and their associated percentiles are useful only if they pertain to the non-noise component of the histogram, hereafter called the *signal distribution*. In fact, the 90th percentile of the histogram shown in Figure 2 is near the right-most hump and therefore unrealistic. Therefore, to compute useful percentile-based envelopes, one must first disambiguate the signal and noise contributions to the histogram. To that end, here, a gaussian mixture model with 2 components[16,17] was used to represent the noise and signal components, respectively. The component appearing to the left (closest to the origin) was defined as the signal distribution. Armed with the signal distribution, the 3 percentiles were computed at each time, and their time series was computed for 59 patients. The 3 percentile-based envelopes for patient X are shown in Figure 3, both with the spectrogram (top panel), and without (bottom panel).

In this article, the details of this percentile-based approach for estimating an envelope are presented. It was found that the estimates are visually consistent with the underlying spectrograms, and the modified geometric method envelope is approximately consistent with the 95th percentile envelope. Also, it is shown that percentile-based envelopes naturally allow for displaying envelope uncertainty.

Materials and Methods

Data

Patient data for this preclinical study were collected from a variety of hospitals in the United States, following a study at the University of Washington led by Dr Mourad. The data included arterial blood pressure and intracranial pressure, but those data were not used for this study; only sonographically derived transcranial Doppler spectra were used. Further details on the patient data may be found in an article by Marzban et al.[18] In accordance with the Institutional Review Board for each hospital, informed consent was obtained from all patients or their families.

Doppler spectral time series of blood flow speed in the middle cerebral artery (or flow velocity – flow velocity) were acquired at each institution via clinically approved transcranial Doppler units. Data acquisition lengths varied from 5 to 30 minutes. All retrospective data processing and

analysis were conducted at the Applied Physics Laboratory of the University of Washington. Doppler spectral time series data collected via the Applied Physics Laboratory's hospital cohort were initially digitized at 125 Hz in time and with a frequency resolution of 128 Hz at a given time. We then down-sampled these Doppler time series to a resolution of 40 Hz in time, sufficient to resolve all of the following features in all of our patients' data: systolic rise, diachrotic notch, and diastolic minimum. We also selected a fixed duration (118 time steps, or ≈3 minutes) from each of the 59 patients for statistical analysis. This duration was sufficiently long to include several cardiac cycles while still allowing details of the envelopes to be visually evident.

Data Processing and Statistical Analysis

As mentioned in the introduction, the main aims of the proposed method were to first represent the instantaneous Doppler frequency distribution of the flow velocity at a given moment in time and then to produce spectral envelopes of those frequency distributions through time based on percentiles of that distribution in the Doppler frequency. Distinguishing the signal from the noise requires a model. In this article, it is assumed that the underlying distribution of flow velocity consists of 2 distributions, corresponding to the signal and noise, and that both are gaussian. This type of model is a special case of gaussian mixture models, wherein a distribution is assumed to be a linear combination of gaussian distributions.[16,17] The weights in the linear combination (called mixing proportions) and the parameters of the gaussian distributions are then estimated from data via some optimization procedure. (In this study, the expectation-maximization algorithm was used, but other parameter estimation methods are equally adequate. The expectation-maximization algorithm maximizes the conditional expected log likelihood.[19]) Figure 4 shows the signal component (black) and the noise component (red) for the example shown in Figure 2. Also shown are the locations of the maximum flow velocity according to modified geometric method (black vertical line) and the 90th, 95th, and 99th percentiles of the signal distribution (blue vertical lines). All statistical analyses were performed in R.[20]

Results

The previous section illustrates the proposed method on a given patient and at a given time. The top panel in Figure 3 shows the 3 percentile-based envelopes (blue curves) for patient X. It is evident that the percentile-based envelopes are consistent with the underlying spectrogram. The bottom panel in Figure 3 shows 4 envelopes; the modified geometric method envelope (black) is comparable with the 95th percentile envelope (red), sandwiched between the 90th and 99th percentile envelopes (blue). Clearly, displaying multiple percentile-based envelopes conveys a sense of the uncertainty in the maximum flow velocities.

Although technical, it is also worth mentioning 2 additional steps taken to generate the percentile-based envelopes shown in Figure 3: (1) The optimization algorithm used for the gaussian mixture model requires initial estimates of the parameters of interest. At time 0, the initial values of the parameters are assigned randomly, and the optimization algorithm produces parameter values that characterize the 2 best-fit gaussian components of the flow velocity histogram at that time. At all "future" times, the initial values of the parameters are set to the final values obtained at the previous time step. This process allows some of the serial (auto) correlation in the spectrogram to be reflected in the envelopes. If the values of the gaussian mixture model parameters are initialized randomly for every and all time steps, the resulting envelopes are somewhat less smooth than those shown in Figure 3. (2) A running-median filter with a window size of 3 seconds is applied to the envelopes to smooth them even further. The size of the window (ie, 3) is obtained by trial and error and by a visual comparison with the modified geometric method envelope. The modified geometric method envelope too is smoothed by a variety of techniques, eg, an averaging (over multiple cardiac cycles) filter and a finite impulse response

Figure 4. Histogram of flow velocity (FV) for patient X (circles) and the estimated densities for the 2 gaussian components. The black vertical bar denotes the maximum flow velocity according to the modified geometric method, and the blue vertical bars correspond to the 90th, 95th, and 99th percentiles of the signal distribution on the left.

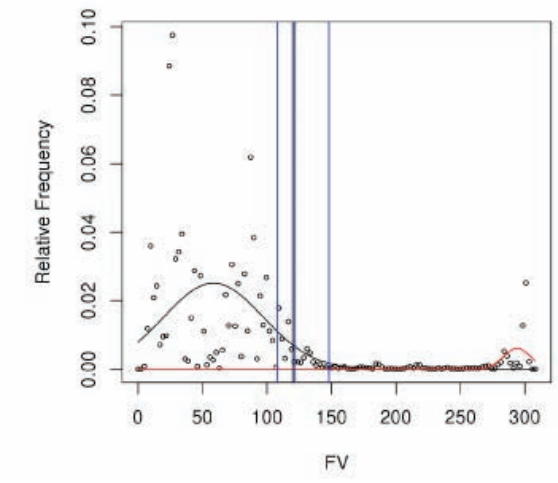

Author: On Figure 5, please verify patient X as changed from Spencer.

filter. Although the smoothness of the displayed envelopes is important in a clinician's decision making, it is a feature that is easily controlled (eg, by a single parameter, such as the window size of the running-median filter) and so is not of serious concern.

The procedure was applied to all 59 patients in the data set. It is impractical to show all 59 figures analogous to Figure 3. Instead, the 3 percentile-based envelopes were compared with the modified geometric method envelope using scatterplots, which were then further summarized into scalar measures.

Each panel in Figure 5 shows the scatterplot of one of the percentile-based envelopes versus the modified geometric method envelope for patient X. There are 118 points on each scatterplot, corresponding to the 118 time steps displayed in Figure 3. The diagonal line is simply a line of slope 1, y-intercept 0. It is clear from the middle panel that the 95th percentile envelope generally agrees with the modified geometric method envelope. As expected, the 90th and 99th percentile envelopes are generally lower and higher, respectively, than the modified geometric method envelope. The disagreements between the percentile-based envelopes and the modified geometric method envelope are largest for higher flow velocity values. This result is especially evident in the 99th percentile envelope (bottom panel) in the manner in which the deviation of the scatterplot from the diagonal line is largest for higher flow velocity values. In other words, the systolic peaks of the 99th percentile envelope are in fact higher than might be expected from the modified geometric method envelope.

One may further summarize each of these panels by computing the root mean squared error between the modified geometric method envelope and each percentile-based envelope. For patient X, the root mean squared error values corresponding to the 3 panels in Figure 5 are 17.9, 16.9, and 31.2 cm/s. In addition to confirming that the modified geometric method envelope is closest to the 95th percentile envelope (for patient X), these numbers have useful interpretations as well; eg, it can be said that the modified geometric method envelope and the 95th percentile envelope have a typical deviation of about 16.9 cm/s across the 118 time steps examined.

Although useful for comparing different envelopes, root mean squared error values do not assess whether the difference in the envelopes is due to the amount of scatter in the scatterplot or to an overall shift. There exists a decomposition of root mean squared error that allows one to examine both contributions. The details of the decomposition are presented in "Appendix." Here, suffice it to say that the correlation coefficient (denoted Corr) and bias (ie, mean [modified geometric method] – mean [percentile-based method]) gauge the amount of scatter and the overall shift, respectively. The Corr values for the 3 panels in Figure 5 are 0.80, 0.81, and 0.81 (from top to bottom), suggesting that the amount of scatter in the 3 panels is comparable. Said differently, any of the 3 percentile-based envelopes provides an adequate approximation to the modified geometric method envelope, if/when correlation is the measure of agreement. The main difference between the 3 panels is in the Bias values: 8.5, –2.6, and –23.5 (from top to bottom). These numbers have useful interpretations, too; eg, one can say that the 95th percentile envelope is generally shifted above the modified geometric method envelope by about 2.6 cm/s for patient X.

To compare the various envelopes across all of the patients, root mean squared error, Corr, and Bias were computed for all 59 patients. Their distributions are shown in Figure 6. The left-most box plot in the top panel summarizes the histogram (across 59 patients) of the root mean squared error computed for the 90th percentile envelope and the modified geometric method envelope (across 118 time steps).

The middle panel in Figure 6 is analogous to the top panel except that the measure of agreement between the modified geometric method envelope and the percentile-based envelope is Corr. The 3 box plots are comparable, implying that all 3 percentile-based envelopes are comparably correlated with the modified geometric method envelope across all 59 patients. The bottom panel shows that, on average (across all 59 patients), the 90th and 99th

Figure 5. Scatterplots of the 3 percentile-based envelopes and the modified geometric method envelope for patient X. FV indicates flow velocity.

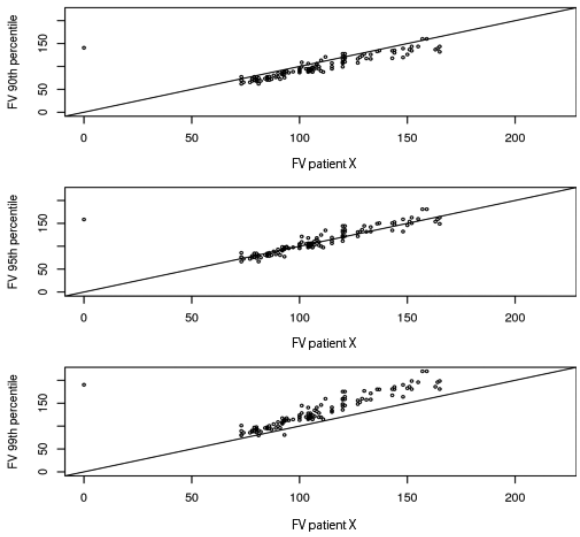

percentile envelopes are below and above the modified geometric method envelope, respectively. By comparing the 3 box plots in the top or bottom panel, it can be seen that the agreement between the modified geometric method envelope and the 95th percentile envelope, noted for patient X, extends to all 59 patients.

It is worth displaying the envelope for a patient for whom such scalar measures are generally poor. Figure 7 shows the spectrogram and envelopes for the patient with the lowest Corr value. It is clear that the modified geometric method envelope (black) is in fact incorrect and that the percentile-based envelopes (blue) are more consistent with the underlying spectrogram. In other words, the low Corr value for this patient does not imply a defect on the part of the percentile-based envelope but rather a defect in the modified geometric method envelope.

Discussion

It has been shown that a double-gaussian mixture model can be used to identify a component of the histogram of flow velocity corresponding to a "signal." In turn, percentiles of this signal distribution provide envelopes, which meaningfully quantify the largest flow velocity. Not only are these percentile-based envelopes visually consistent with their underlying spectrograms, they are also objectively consistent with a commonly used envelope based on the modified geometric method. The percentile-based envelopes not only objectively quantify what is meant by "largest flow velocities" but also have the added advantage (over existing envelopes) of allowing for a natural display of uncertainty in the envelopes.

Given that the analysis is performed on real (not simulated) data, the true envelope is not known. As such, the quality of each envelope cannot be assessed objectively on its own merit. For that reason, the analysis here has been based on visually comparing an envelope with the underlying spectrogram (eg, as in Figure 3), or objectively comparing each of the percentile-based envelopes with the modified geometric method envelope (eg, Figures 5 and 6). In spite of the central role played by the modified geometric method envelope in comparing envelopes, it is important to recall that the modified geometric method envelope is not the true envelope (eg, see Figure 7). Here, it is used as a standard only because of its common usage.

Of the 3 percentile-based envelopes, the 95th percentile envelope is closest to the modified geometric method envelope, but the agreement is not perfect, as seen by the box plots in Figure 6. For example, according to the middle box plot in the bottom panel, on average (across patients), the 95th percentile envelope is slightly above the modified geometric method envelope. One may ask what is the exact percentile corresponding to the modified geometric method envelope, but the question itself is inappropriate because it elevates the status of the modified geometric method envelope to a "reference standard," when in fact it is not. What is more important is that the proposed approach produces a useful spectrogram as well

Figure 6. Distribution of the root mean squared error (RMSE), correlation coefficient (Corr), and Bias (defined in "Appendix") for all 59 patients examined in this work.

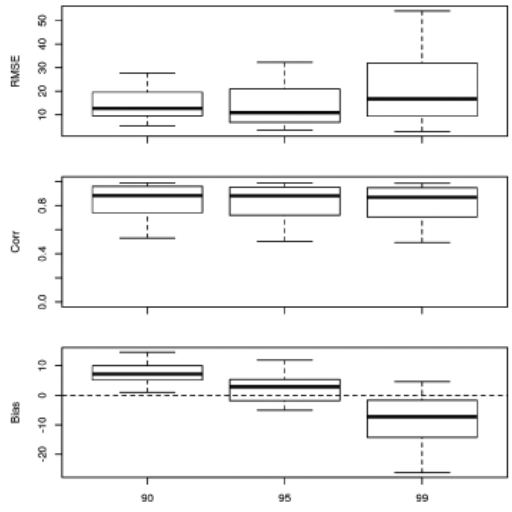

Figure 7. Same as Figure 3, but for a patient for whom the modified geometric method envelope (black) is clearly incorrect. FV indicates flow velocity.

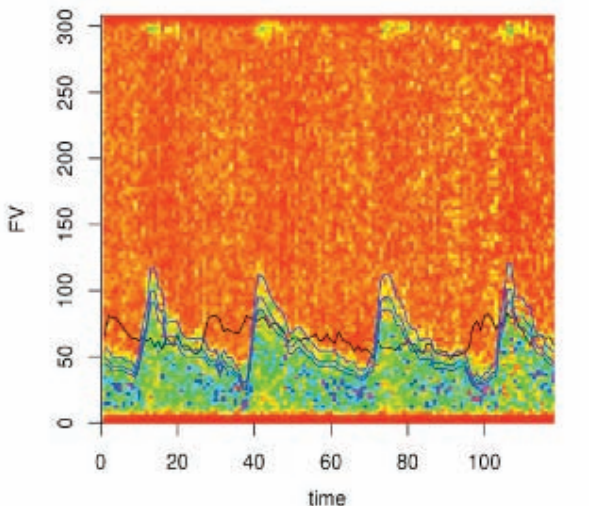

as an interpretable (in terms of percentiles) generalization of approaches that naturally produce only a single envelope (eg, modified geometric method).

A percentile-based envelope is based on a percentile of the signal distribution, in which the signal (and noise) distribution is defined from fitting a gaussian mixture model with 2 components to the whole histogram, at a given time. There is some justification for examining the 3 components. For example, in Figure 4, one may argue that there are possibly 3 overlaying histograms: 1 corresponding to the large hump on the left (ie, the signal), 1 associated with the small hump on the right (ie, associated with an aliasing reflection on Doppler imaging, and another corresponding to a uniform "background" spanning the full range of flow velocity values. We repeated the entire analysis but with 3 gaussian components. The results are inconclusive and require further research. For some patients, the results do not change substantially, but for others, they do in ways that can be considered "better" or "worse" depending on the measure of quality.

The percentiles of the signal distribution allow for meaningful envelopes, which can objectively assess the largest flow velocity. In addition, displaying multiple envelopes can convey information on the uncertainty in the observed flow velocity. One can envisage an alternative measure of uncertainty. For example, one may consider the envelope corresponding to a fixed percentile, say 95th, and then obtain the distribution of that quantity via some resampling method.[21] In turn, that (sampling) distribution can be used to compute confidence intervals for the true 95th percentile envelope. Such interval estimates of the envelope can be useful in conveying uncertainty if/when a specific percentile is of interest. Otherwise, displaying multiple envelopes corresponding to different percentiles, as done here, is sufficient for conveying uncertainty.

Appendix

Let x_i and y_i denote the values of the modified geometric method envelope and a percentile-based envelope, respectively, at time i. The root mean square error between 2 envelopes is defined as the square root of the mean square error (MSE):

$$(1) \qquad MSE = \frac{1}{n-1} \sum (y_i - x_i)^2,$$

where n is the length of the time steps (here, 118). It can be shown that

$$(2) \qquad MSE = s_x^2 + s_y^2 - 2(\mathrm{Corr}) s_x s_y + \frac{n}{n-1} (\mathrm{Bias})^2,$$

where s_x and s_y are the sample standard deviations of x and y, respectively, Corr denotes the Pearson correlation coefficient, and

$$(3) \qquad \mathrm{Bias} = \mathrm{mean}\ x - \mathrm{mean}\ y.$$

According to Equation 2, a comparison of 2 envelopes in terms of mean square error (or root mean square error) is equivalent to a comparison in terms of Corr and in terms of Bias; the former compares the correlation between the envelopes, and the latter measures the overall shift between them.

References

1. Sloan MA, Wozniak MA, Macko RF. Monitoring of vasospasm after subarachnoid hemorrhage. In: Babikian VL, Wechsler LR, Toole JF (eds). *Transcranial Doppler Ultrasonography*. Boston, MA: Butterworth-Heinemann; 1999:109–128.
2. Aaslid R, Nornes H. Musical murmurs in human cerebral arteries after subarachnoid hemorrhage. *J Neurosurg* 1984; 60:32–36.
3. Aaslid R, Huber P, Nornes H. Evaluation of cerebrovascular spasm with transcranial Doppler ultrasound. *J Neurosurg* 1984; 60:37–41.
4. Aaslid R, Huber P, Nornes H. A transcranial Doppler method in the evaluation of cerebrovascular spasm. *Neuroradiology* 1986; 28:11–16.
5. Aaslid R. Transcranial Doppler assessment of cerebral vasospasm. *Eur J Ultrasound* 2002; 16:3–10.
6. Oertel M, Boscardin WJ, Obrist WD, et al. Posttraumatic vasospasm: the epidemiology, severity, and time course of an underestimated phenomenon—a prospective study performed in 299 patients. *J Neurosurg* 2005; 103:812–824.
7. Armonda RA, Bell RS, Vo AH, et al. Wartime traumatic cerebral vasospasm: recent review of combat casualties. *Neurosurgery* 2006; 59:1215–1225.
8. Babikian VL, Wechsler LR, Toole JF (eds). *Transcranial Doppler Ultrasonography*. Boston, MA: Butterworth-Heinemann; 1999.
9. Tsivgoulis G, Alexandrov AV, Sloan MA. Advances in transcranial Doppler Ultrasonogrphy. *Curr Neurol Neurosci Rep* 2009; 9(1):46-54.
10. Tegeler CH, Rotanakorn D. Physics and principles. In: Babikian VL, Wechsler LR, Toole JF (eds). *Transcranial Doppler Ultrasonography*. Boston, MA: Butterworth-Heinemann; 1999:3–11.
11. Moraes R, Adin N, Evans DH. The performance of three maximum frequency envelope detection algorithms for Doppler signals. *J Vasc Invest* 1995; 1:126–134.
12. Fernando KL, Mathews VJ, Clark EB. A mathematical basis for the application of the modified geometric method for maximum frequency estimation. *IEEE Trans Biomed Eng* 2004; 51:2085–2088.
13. Güler I, Hardalaç F, Kaymaz M. Comparison of FFT and adaptive ARMA methods in transcranial Doppler signals recorded from the cerebral vessels. *Comput Biol Med* 2002; 32:445–453.

14. Östlund N, Yu J, Karlsson JS. Improved maximum frequency estimation with application to instantaneous mean frequency estimation of surface electromyography. *IEEE Trans Biomed Eng* 2004; 51:1541–1546
15. Rubin JM, Bude RO, Fowlkes JB, Spratt RS, Carson PL, Adler RS. Normalizing fractional moving blood volume estimates with power Doppler US: defining a stable intravascular point with the cumulative power distribution function. *Radiology* 1997; 205:757–765.
16. McLachlan GJ, Peel D. *Finite Mixture Models*. Hoboken, NJ: John Wiley & Sons; 2000.
17. Bishop C. *Pattern Recognition and Machine Learning*. New York, NY: Springer; 2006.
18. Marzban C, Illian PR, Morison D, et al. A method for estimating zero-flow pressure and intracranial pressure. *J Neurosurg Anesthesiol* 2013; 25:25–32.
19. Dinov ID. Expectation maximization and mixture modeling tutorial. California Digital Library, Statistics Online Computational Resource website; December 9, 2008. http://repositories.cdlib.org/socr/EM_MM.
20. R Development Core Team. R: a language and environment for statistical computing. R Project website; 2011. http://www.R-project.org.
21. Efron B, Tibshirani RJ. *An Introduction to the Bootstrap*. London, England: Chapman & Hall; 1998.

A Model of Blood Flow based on Transcranial Doppler Ultrasound

David Morison,Caren Marzban, Pierre D. Mourad

September 19, 2013

Abstract

A physiological model of blood flow in the middle cerebral artery is put forth. The model consists of a simple circulatory system, pulsatile flow in an elastic tube, and the conversion of flow velocity to spectrograms which can in turn be compared to data. Many of these component models have parameters which are estimated by measurements of blood flow with transcranial Doppler ultrasound. In addition to producing spectrograms which closely resemble observed spectrograms, the model provides a physical basis for the interpretation of spectrograms.

1 Introduction

Modeling blood flow has been a topic of extensive research (refs??). It is important not only for the purpose of understanding the underlying dynamics (refs??), but also for its diagnostic value (refs??). Pierre??

Transcranial Doppler Ultrasound (TDU) provides one method for measuring blood flow (refs??). The measurements are generally displayed in the form of a spectrogram. A spectrogram is a measure of the intensity of acoustic return to TDU as a function of time and velocity, where velocity is derived from signal processing to extract the return due to a velocity toward the transducer. A spectrogram is a function of time in the sense that it is

recorded over time. Such spectrograms, however, are generally corrupted by a number of errors, including measurement errors, return from unwanted sources, etc. Pierre?? A basic assumption in examining Flow Velocity (FV) data is that there exists an underlying spectrogram which adheres to certain physical constraints. For example, at a given time, the brightness/amplitude of a spectrogram is expected to drop to zero at a well-defined (maximum) FV value; but observed spectrograms, usually do not reflect that physical requirement. Also, observed spectrograms are often contaminated by random noise, i.e., random errors which cannot be attributed to any physical constraints. A physics- (or physological)-based model is required to allow one to attribute physical meaning to an observed spectrogram.

The approach proposed in this paper involves both statistical and physical models. Statistical models usually involve parametric, mathematical expressions whose structure is dictated by the convenience of estimating their parameters. Regression models are canonical examples of such models (refs ??; Marzban et al. 2013). By contrast, physical models begin with physiologically-relevant components whose mathematical properties are well-understood, and attempt to describe the overall phenomenon (e.g., blood flow) by an assembly of such components.

Physiologically based blood flow models of the type examined here have been considered in the past, but the model parameters have not been estimated from an entire spectrogram (refs??). For example, [15] et al. model blood flow through a constriction, but at no stage in that work a spectrogram is used to estimate the model parameters. By contrast, when a spectrogram is fully employed, the focus of the work is an envelope, and not a 2d flow velocity field (refs?? geo method, double-gaussian ...??). One novel feature of the proposed method is the manner in which a full physiologically-based blood flow model is utilized, and its parameters are estimated from an entire spectrogram. The estimation method, a simple instance of *Recursive Bayesian Estimation* (RBE), (refs??) involves iteratively making observations, and revising estimates about the system from which those observations originate. RBE has been proven useful in a wide range of applications (refs??, include subs), including the modeling of blood flow [4] (more refs??).

Note to self: Cite Windkessel model as in [2].??

The flow chart in Figure 1 highlights the major components of the methodology.

First, an observed spectrogram is consulted in order to choose initial values for some parameters. These values are then used in a model of the circulatory system, which in turn produces a one dimensional time series of maximum FV. Solutions to approximations of Navier Stokes equations in an elastic tube are used to convert the 1-D time series into a 2-D flow field. Although the modeled axial and radial flow velocity and vessel wall motion can be used for multiple purposes, the main attribute of interest is the (ideal) spectrogram computed from it. All of the component models which lead to this ideal spectrogram are referred to as the forward model. The ideal spectrogram is then compared to the observed spectrogram, the result of which is a posterior Probability Density Function (PDF) of some of the parameters, given an observed spectrogram. From this PDF, optimum values for some of the parameters are obtained. From the entire model a number of clinically useful quantities can be generated, such as envelope, mean flow, or pulsatility index. The complete process of estimating the dynamic and fixed parameters is often referred to as inverting the forward model.

2 Data

Ninety six recorded spectrograms are examined, 73 of which are collected with the Spencer Technologies TDU device in a hospital setting. The majority of these patients have experienced traumatic brain injury, and five have exhibited vasospasm. The spectrograms for the remaining 23 patients are from a Presto TDU device currently under development. Pierre??

The spectrograms for the 96 patients are complex and varied across patients. Although the spectrogram for each patient appears to be consistent with what one might expect from an ideal spectrogram, no simple ideal spectrogram emerges as a viable candidate when multiple patients are examined. In fact, the spectrograms for 9 of the 73 patients are sufficiently complex to have failed a commonly-used envelope-detection algorithm, referred to as the modified geomteric algorithm [12].

Figure 2 shows the spectrogram as measured by a TDU device (spencer or

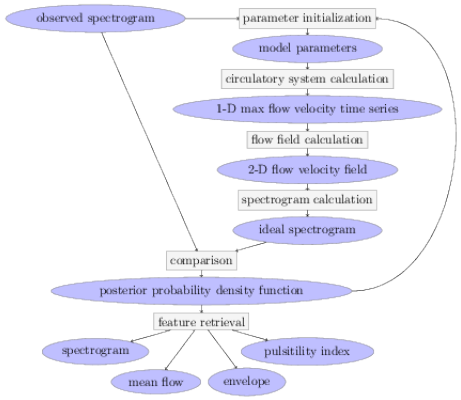

1

Figure 1: In the proposed methodology the forward model consists of several components, each with parameters which are to be estimated from observed spectrograms. The parameters are randomly initialized, and the resulting output of the forward model is compared with an observed spectrogram. An RBE approach is then employed to update the parameters, with the goal of improving the agreement between observed and predicted spectrograms.

presto??). Note the varying shading in the "body" (i.e., the lower portion) of the spectrogram, in contrast to the relatively constant "background" (middle portion). The top portion is due to aliasing, and will be further discussed, below. Also, note the characteristic systolic peak and dicrotic notch. It is important to note that the amplitudes shown in this figure are all on logarithm scale. Indeed, all of the following analysis is performed on the logarithm

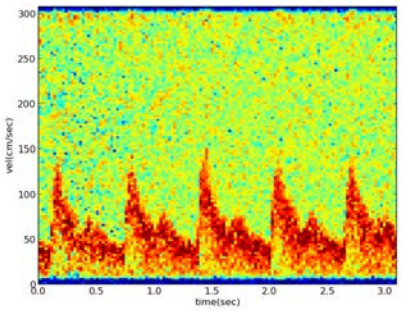

Figure 2: The observed spectrogram for one patient.

of the observed spectrogram amplitude. The logarithmic transformation is motivated by the empirical result that the logarithm of the amplitudes is bell-shaped.

3 Methods

In this section details of the flowchart (Fig. 1) are described.

3.1 Parameter Intialization

The data collected as a spectrogrm are over the domain of time and doppler velocity. We develop a model on the domain of two independent variables, heart rate and phase within a cardiac cycle. The model is posed this way because it is assumed that the system of interest may be approximated at any instant in time by a perfectly periodic system. The interval of idealized periodicity is called a cardiac cycle. The phase, θ, of an event specifies the time at which that event occurs within a cardiac cycle. Heart rate, ω, is the number of cardiac cycles that would occur per unit time in the perfectly periodic approximation. The time evolution of θ and ω are related and assumed to be stochastic. The usual relation between the two independent variables, namely $\frac{d\theta}{dt} = \omega$ will be posed as a transition probability in a markov

chain model of dynamic variables within the RBE.

Each of the components of the proposed model introduces a number of parameters (Table 1), which are treated in two different ways. The values of most of the parameters are fixed in time for a given patient, and are optimized over the entire time interval of the patient's observed spectrogram. Two of the parameters, however, are not only dynamic in that they are allowed to vary in time, their possible values are determined *a priori* over a grid. The grid coordinates are the values of the two dynamic parameters and are the phase within a cardiac cycle, θ, and heart rate, ω. As a result, at any time, the aforementioned pdf is a function over these two dynamic parameters.

3.2 Circulatory System Calculation

A simple Windkessel model, i.e. an electric circuit analogy, is used to produce a time series of total flow, or of some other gross property of flow. The nonlinear circuit illustrated in Fig. 3.2 exhibits a variety of realistic wave forms when it is driven by a square wave.

James, This is one place where we can use your help. The bottom circuit diagram is what I have been working with. However, the results don't look too good. I will continue working on it, but because of time constraints I had to find something that does work. The top diagram seems to work OK. So, the question for you is whether you can impose a physiological interpretation on the top/simple diagram? For the longer term, we can explore other diagrams too, but for now I'm stuck with just these two.

The circuit is a rough analogy to a single-chambered heart driving circulation through a simple resistive body. The heart in this model consists of a lone ventricle with inlet and outlet valves, and an aorta. The body consists of a single resistor representing all arteries, capillaries, veins, etc. The action of the ventricle is represented as a voltage source with a relatively high output impedance. The valves are modeled as Shockley diodes with finite resistance and compliance, representing the drag as blood moves through the valves and the oscillation of the valve membrane. The aorta is assumed to be elastic, and the blood flowing into it is assumed to have some momentum. A simple resistor represents the flow through the body.

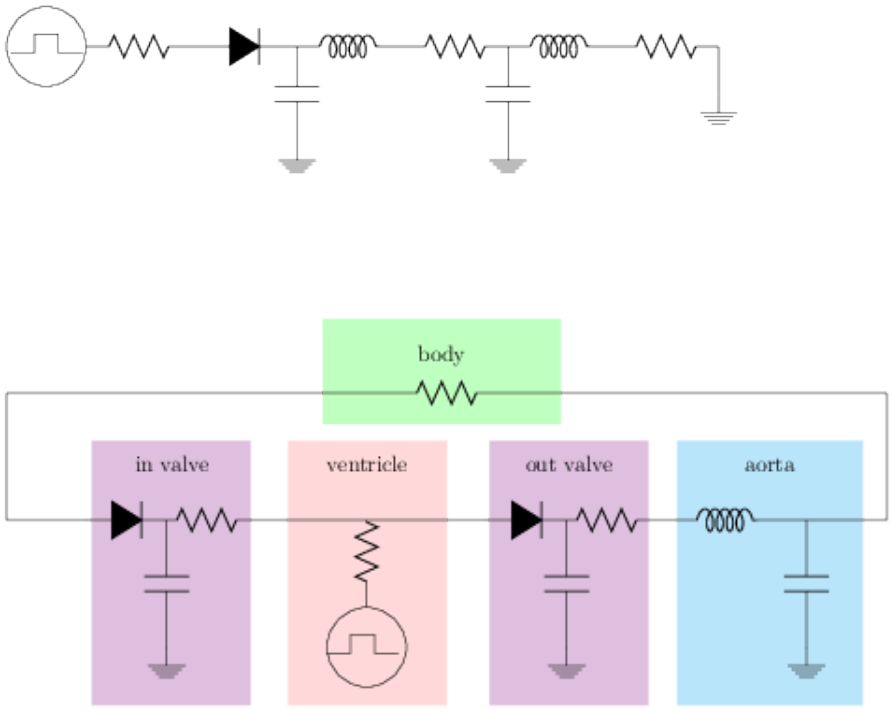

Figure 3: Two circuit diagrams.

The presence of the diodes is essential in assuring realistic flow wave forms. Without the diodes in Fig. 3.2 the problem is linear, and so, can be solved by computing a transfer function mapping the driving square wave to the corresponding current through the body resistor, but important features would be missing from the resulting wave form. With diodes the current through the resistor is dictated by a system of first order differential equations, which can be solved numerically.

The twelve parameters associated with the various components in the circuit analogy are tabulated in Table 1. Two of these parameters - heart rate (ω), and phase in cardiac cycle (θ) - are dynamic, while the remaining ten are fixed.

parameter	symbol	notes about prior
heart rate	ω	gridded
phase in cardiac cycle	θ	gridded
diode saturation current	s	lognorm
diode exponent coeff	k	lognorm
capacitance of valve	c_v	lognorm
resistance of valve	r_v	lognorm
inductance of aorta	l_a	lognorm
capacitance of aorta	c_a	lognorm
source impedence	r_h	lognorm
source voltage	v_0	lognorm
square wave width	$dwell$	lognorm
resistance of body	r_b	lognorm

Table 1: The dynamic and fixed parameters introduced in the Circulatory System Calculation component of the model.

For each gridded value of the dynamic parameters the circuit simulation is run for a sufficiently long time so as to remove transient behavior. As such, the entire circuit model may be represented as a gridded function $f(\omega, \theta)$, where each gridded value corresponds to a maximum flow velocity.

Fig. 3.2 shows the time series of maximum flow velocity for the patient whose spectroram is shown in 2. These time series has some desirable features, such as the presence of a dicrotic notch, the realistic relative scale

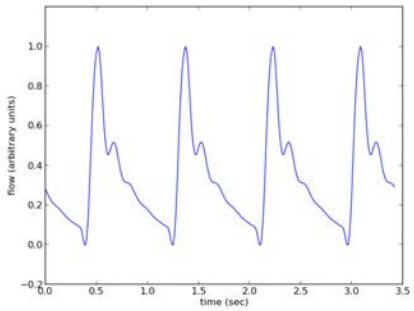

Figure 4: An example of the time series of maximum flow velocity produced by the circuit shown in Figure 3.2

between the dicrotic notch and the systolic peak, and the qualitative "exponential" decay following the peak. Pierre, James, do you want to say more about this figure??

3.3 Model of Flow in the Middle Cerebral Artery: Flow Field Calculation

The aforementioned windkessel model produces a time series of total flow through the artery. This 1-D time series is then used as a boundary condition which the flow velocity field solutions must satisfy in the flow field model.

In the flow field calculation the middle cerebral artery is modeled as an elastic tube ([3] and [5]). The tube is assumed to be straight; this assumptions is reasonable because although the middle cerebral artery is convoluted, the typical radius of curvature along the artery is larger than the radius of the artery itself. The vessel wall is assumed to be thin, allowing one to treat it as a Hookean membrane[1].

The mathematical details of this model are similar to that developed in Chapter 17 of [1]. Specifically, beginning with Equations 17.128, 17.129, and 17.131 it is straightforward to show

$$0 = Q_a k^2 + Q_b k + Q_c, \tag{1}$$

$$Q_a = \frac{1-\hat{v}/2}{\beta\omega}\left(\frac{-iEh}{\omega^2\rho a_0^2}\right) - \frac{Eh}{2\rho a_0\omega^2}\frac{-i}{\omega}\left(\frac{j_0\left(\hat{\beta}\right)}{j_1\left(\hat{\beta}\right)} - \frac{\hat{v}}{\hat{\beta}}\right), \tag{2}$$

$$Q_b = \frac{1-\hat{v}/2}{\beta\omega}\frac{i\hat{v}}{a_0}\frac{-Eh}{2\rho a_0\omega^2}(\hat{v}^2-1)\frac{\beta\mu}{Eh} + \frac{-i}{\omega}\left(\frac{j_0\left(\hat{\beta}\right)}{j_1\left(\hat{\beta}\right)} - \frac{\hat{v}}{\hat{\beta}}\right), \tag{3}$$

$$Q_c = \left(\hat{v}^2-1\right)\frac{\beta\mu}{Eh} \tag{4}$$

where ?? make sure all the symbols are defined.?? The reason these questions are derived here is that equations 17.134 and 17.135 in [1] are erroneous.[1]

The vessel wall and fluid velocity solutions are required to satisfy the following conditions. The flow through the artery is assumed to be pulsatile, and we seek solutions for radial and axial velocities of the form $v(r,t)$ and $u(r,t)$, where r is the distance from the axis. As such, the solutions are rotationally symmetric, and there is no angular velocity. Furthermore, the fluid is assumed to be incompressible and satisfying the Navier-Stokes equation.

Flow fields like this have been studied by [3] and [5], and solutions are a current area of research, for example in [6] and [15]. Solutions are generally obtained through Fourier decomposition of the forcing. In order to arrive at analytic solutions, certain approximations are made, which in turn allow for two modes (i.e. types of solutions) to exist for each harmonic [1]. The most general solution, a combination of these two modes, therefore requires two parameters to be specified uniquely. The two parameters are taken to be the phase and amplitude at each frequency. The relative phase and relative amplitude of the two modes are assumed to be constant in frequency and time. These values are constrained to assure an agreement between the solution and the 1-D time series produced by the circulatory system model. For a frequency zero (steady state) component it is assumed that the axial flow is a Hagen-Poiseuille (parabolic) type, and there is no radial flow. [2]

[1] ?? Do we need to derive this??

[2] extending the pulsitile solution a steady state solution would be inconsistent with the

The basic physical equations defining the flow field model [1] involve the fixed parameters in table 2.

parameter	symbol	notes about prior
density of blood	ρ	?
viscosity of blood	μ	?
density of vessel wall	ρ_w	?
equilibrium radius of vessel	a	?
thickness of vessel wall	h	?
Possion's ratio of vessel wall	υ_w	?
Young's modulus of vessel wall	E	?
relative amplitude of "+" mode	X_+	the complex ratio between the two modes
relative amplitude of "-" mode	X_-	might be considered four real numbers

Table 2: The fixed parameters introduced in the Flow Field Calculation component of the model.

As seen in Fig. 3.3, the lowest Womersley number (top row) modes resemble a combination of Hagen-Poiseuille flow and solid vibration. Note that as the frequency increases, the shape of the axial flow velocity becomes increasingly complex for the "minus" mode (top panel), and the radial component grows in the "plus" mode (bottom panel).

The output of model of blood flow in the middle cerebral artery is shown in Fig. 3.3. The axes are radius and time, with the axial velocity shown parallel to the time axis. Typically, the radial velocity is on the order of 100 to 200 times less than the axial velocity; here, they have been scaled to achive visual clarity. It may be tempting to ignore the lower amplitude radial component in favor of the higher amplitude axial component; however, because the observed spectrograms span the full domain of velocity, including near-zero velocity, the scale disparity between the two components does not justify discarding the lower amplitude velocities.

premise of that flow model. In this simple iteration nothing is holding the vessel in place other than symmetric forcing.

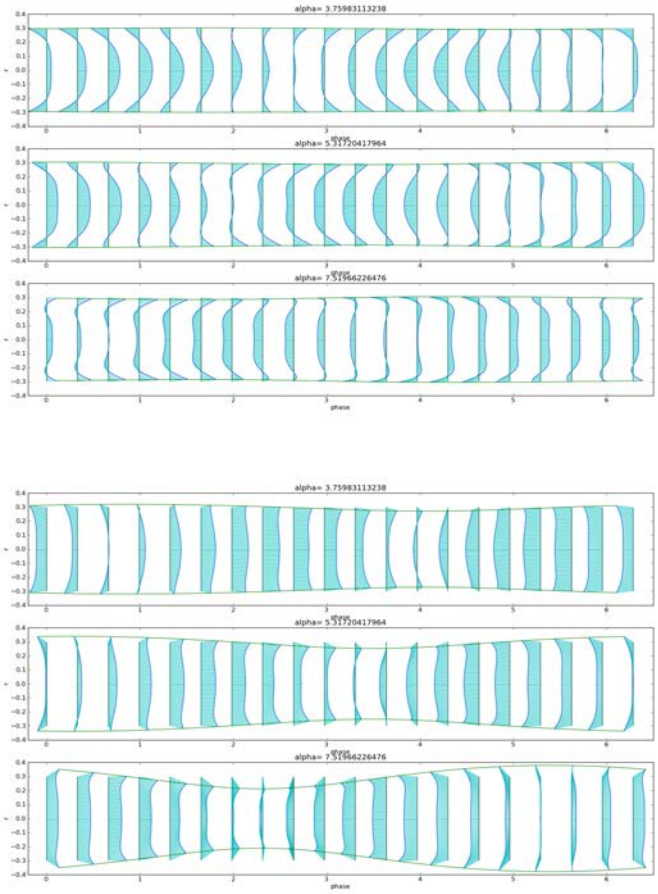

Figure 5: An example of the two degenerate modes of wave propogation. The top (bottom) panel corresponds to the "minus" ("plus") mode, and the three rows in each panel correspond to three values of Womersley number in order of increasing frequency from top to bottom.

3.4 Model of Transcranial Doppler Ultrasound: Spectrogram Calculation

The preceding steps in the proposed model produce a 2-D flow velocity field. TDU, however, produces a spectrogram, i.e., a time series of the histogram of

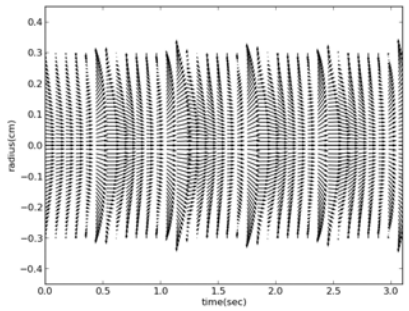

Figure 6: The output of model of blood flow in the middle cerebral artery.

the volume corresponding to a doppler velocity v (where volume refers to the total number scatterers [10]). In order to compare this simulated blood flow velocity field to the observed doppler ultrasound, therefore, a spectrogram must be derived from the modeled velocity field.

The TDU considered here interrogates only the flow velocity field component along the transducer axis. Though the simulated blood flow is axisymmetric the transducer is not assumed to be aligned with the middle cerebral artery. Introducing an off bore angle Φ, the speed toward the transducer v' is given by

$$v'(r, \phi, \Phi) = v_{axial}(r) \cos\Phi + v_{radial}(r) \sin\Phi \cos\phi \quad , \tag{5}$$

with ϕ the angle in cross section of the artery. Said differently, in a cylindrical coordinate system aligned with the artery r, ϕ and z, ϕ is the polar angle (around the symmetry axis of the artery), and Φ is difference in angle between the symmetry axis of the ultrasond foucs and the artery. This doppler velocity v' is a function of the corridnate system of artery. An ideal spectrogram will some measure this v' but the spectrogram itself is a function of v. An ideal spectrogram is a measure of how much volume within the focus area is moving at a velocity v; i.e., for what area in the coordinate system of the artery is $v' = v$. Denoting (r, ϕ) with $\vec{x}$, and supressing Φ, an ideal spectrogram $s_{ideal}(v)$ can be defined as

$$s_{ideal}(v) = \lim_{\epsilon \to 0} \frac{1}{2\epsilon} \text{Area in } \vec{x} \text{ such that } |v'(\vec{x}) - v| < \epsilon \tag{6}$$

Said differently, the ideal spectrogram is the infinitesimal area for which the doppler component of the flow velocity field is equal to the ideal spectrogram velocity. It is relatively straightforward to show that for a broad class of v', the limit in equation 6 can be written as

$$s_{ideal}(v) = \oint_{v=v'} \frac{dl}{|\nabla v'|} \tag{7}$$

Where l is any parameterization of contours for which $v'(\vec{x}) = v$. The relationship between an ideal spectrogram and a flow velocity field has been studied by Evans [9], but not in integral/closed form as in equation 7.

Additionally, the ideal spectrogram and the observed spectrogram are assumed to be related by the following statistical model

$$s_{data}(v, \theta(t), \omega(t)) = s_{ideal}(v, \theta(t), \omega(t)) f_v(v) + B_0, \tag{8}$$

$$z(v, t) = s_{data}(v, \theta(t), \omega(t)) + N(v, t) \tag{9}$$

where N is a zero mean gaussian random variable, and B_0 is a fixed parameter representing background clutter. The observed spectrogram data is z, and it differs from the rescaled spectrogram s_{data} by the addition of noise N. The variance of N for a given time and spectrogram velocity is chosen a priori during the developement of this statistical model, the covariance of N at differing times and places is assumed to be zero. An initial and a refined estimate of B_0 is made for each outer loop completed in Fig. 1.

parameter	symbol	notes about prior
off bore angle of transducer	Φ	2d norm rayleigh? 30° thing?
reflectivity of blood	B_b	MLE so matters in tracker not in feedback
reflectivity of tissue	B_t	MLE so matters in tracker not in feedback
background clutter	B_0	MLE so matters in tracker not in feedback
variance of noise	σ	MLE so never matters

Table 3: parameters introduced in the Spectrogram Calculation component of the model.

3.5 Recurssive Bayesian Estimation: Comparison

The preceding analysis leads to an ideal spectrogram depending on the value of the dynamic parameters. Within a recursive Bayesian framework the observed spectrogram z is combined with the predicted spectrogram s_{data} to produce a posterior PDF over the dynamic parameters that evolves with time. The location of the maximum value of this posterior PDF is taken as an estimate of the values of the dynamic parameters as they change over time.

The dynamic parameters and the spectrogram are discretized as follows. First, the phase in the cardiac cycle and heart rate are both divided into i time steps: $\theta_i, \theta_{i-1}, ..., \theta_0$ and $\omega_i, \omega_{i-1}, ..., \omega_0$, respectively. The observed spectrogram is a time series $\vec{z_i}, \vec{z_{i-1}}, ..., \vec{z_0}$, where $z\,(j, i)$ is the observed amplitude at the j^{th} doppler velocity and i^{th} time.

All fixed parameters are eponymously fixed and a hypothetical joint distribution over all past and present values of the dynamic parameters and the observed data is considered. The entire state of the system can then be described by a joint PDF of the form

$$P\left(\theta_i, \theta_{i-1}, ..., \theta_0, \omega_i, \omega_{i-1}, ..., \omega_0, \vec{z_i}, \vec{z_{i-1}}, ..., \vec{z_0}\right) \quad . \tag{10}$$

Given that a spectrogram is observed, the relevant quantity is the conditional PDF

$$P\left(\theta_i, \theta_{i-1}, ..., \theta_0, \omega_i, \omega_{i-1}, ..., \omega_0 | \vec{z_i}, \vec{z_{i-1}}, ..., \vec{z_0}\right) \quad . \tag{11}$$

This PDF is a function of past and present values of the dynamic parameters, but the more useful quantity is the PDF of only the latter. Such a PDF can be obtained by marginalizing over all past values of the dynamic parameters:

$$P \quad (\theta_i, \omega_i | \vec{z_i}, \vec{z_{i-1}}, ..., \vec{z_0}) = \tag{12}$$

$$\int \quad P\left(\theta_i, \theta_{i-1}, ..., \theta_0, \omega_i, \omega_{i-1}, ..., \omega_0 | \vec{z_i}, \vec{z_{i-1}}, ..., \vec{z_0}\right) d\theta_{i-1} ... d\theta_0 d\omega_{i-1} ... d\omega_0 \tag{13}$$

which using Bayes' theorem can be rewritten as

$$\int \frac{P\left(\vec{z_i}, ... | \theta_i, ..., \omega_i, ...\right) P\left(\theta_i, ..., \omega_i, ...\right)}{P\left(\vec{z_i}, ...\right)} d\theta_{i-1} ... d\theta_0, d\omega_{i-1}, ... d\omega_0 \quad . \tag{14}$$

The denominator in Eq. 14 contains no parameters, and so, can be ignored.

In order to estimate these PDFs, statistical models are used. Specifically, the first term in the integrand's numerator in Eq. 14 (often called the likelihood) is assumed to be

$$P\left(\vec{z_i}, ...|\theta_i, ..., \omega_i, ...\right) = \prod_{i'=0}^{i} P\left(\vec{z_{i'}}|\theta_{i'}, \omega_{i'}\right) \tag{15}$$

where each of the PDFs in the product is assumed to be multivariate normal with zero means and identical covariances:

$$P\left(\vec{z_{i'}}|\theta_{i'}, \omega_{i'}\right) = N\left(\vec{z_{i'}} - \vec{s_{data}}\left(\theta_{i'}, \omega_{i'}\right)\right) \quad , \tag{16}$$

where the components of the vector $\vec{s_{data}}$ are given by Eq. 8. The product of univariate normal PDFs in Eq. 15 reflects the conditional independence of the observed spectrogram across time. The use of i' rather than i indicates that this relation holds for all values of the time index.

The second term in the integrand's numerator in Eq. 14 (often called the prior) involves only the parameters, and can be written as the product of conditional PDFs involving the value of the parameters at an earlier time step:

$$\begin{aligned} P\left(\theta_i, ..., \omega_i, ...\right) &= P\left(\theta_i, \omega_i|\theta_{i-1}, \omega_{i-1}\right) P\left(\theta_{i-1}, \omega_{i-1}|\theta_{i-2}, \omega_{i-2}\right) ... P\left(\theta_0, \omega_0\right) & (17) \\ &= P\left(\theta_0, \omega_0\right) \prod_{i'=1}^{i} P\left(\theta_{i'}, \omega_{i'}|\theta_{i'-1}, \omega_{i'-1}\right) & (18) \end{aligned}$$

The term $P\left(\theta_0, \omega_0\right)$ is set to a constant.

Each of the PDFs in the product Eq. 18 is assumed to be of the form

$$P\left(\theta_{i'}, \omega_{i'}|\theta_{i'-1}, \omega_{i'-1}\right) = N\left(\omega_{i'} - \omega_{i'-1}\right) V\left(\theta_{i'} - \left(\theta_{i'-1} + \delta_t \omega_{i'-1}\right)\right) \ , \tag{19}$$

where N and V denote the Normal and Von Mises distributions, respectively. The argument of the latter is a reflection of the relationship between the dynamic variables $\omega \approx \frac{d\theta}{dt}$.

Substituting equations 16 and 19 into 15, 18 and then into 14,

$$P\left(\theta_i, \omega_i | \vec{z_i}, \vec{z_{i-1}}, ..., \vec{z_0}\right) \sim \int \left(\prod_{i'=0}^{i} P\left(\vec{z_{i'}} | \theta_{i'}, \omega_{i'}\right) \prod_{i'=1}^{i} P\left(\theta_{i'}, \omega_{i'} | \theta_{i'-1}, \omega_{i'-1}\right) \right) d\theta_{i-1} ... d\omega_{i-1} ... \tag{20}$$

$$= P\left(\vec{z_i} | \theta_i, \omega_i\right) \int \left(\prod_{i'=0}^{i-1} P\left(\vec{z_{i'}} | \theta_{i'}, \omega_{i'}\right) \prod_{i'=1}^{i} P\left(\theta_{i'}, \omega_{i'} | \theta_{i'-1}, \omega_{i'-1}\right) \right) d\theta_{i-1} ... d\omega_{i-1} ... \tag{21}$$

$$= P\left(\vec{z_i} | \theta_i, \omega_i\right) \int \left(\prod_{i'=1}^{i} P\left(\vec{z_{i'-1}} | \theta_{i'-1}, \omega_{i'-1}\right) P\left(\theta_{i'}, \omega_{i'} | \theta_{i'-1}, \omega_{i'-1}\right) \right) d\theta_{i-1} ... d\omega_{i-1} ... \tag{22}$$

$$= P\left(\vec{z_i} | \theta_i, \omega_i\right) \int_{i-1} P\left(\theta_i, \omega_i | \theta_{i-1}, \omega_{i-1}\right) P\left(\vec{z_{i-1}} | \theta_{i-1}, \omega_{i-1}\right) \left(\int_{i-2} ... d\theta_{i-2} d\omega_{i-2} \right) d\theta_{i-1} d\omega_{i-1} \tag{23}$$

The final expression in Eq 23, with the nested integrals depending only on the adjacent values i, is why this method is called recurssive estimation.

The left panels in Fig. 3.5 show the probability of data, given the dynamic parameters (i.e., the likehood), and the right panels display the probability of the dynamic parameters, given data (i.e., the posterior PDF). Note that the likelihood does not appear to have a unique maximum. In particular, there is larger uncertainty in ω than in θ. By contrast, the posterior PDF for one patient (top/right panel) has a unique maximum, and the uncertainty is more in the θ than in ω. The posterior PDF for the other patient (bottom/right) displays at least two modes. Do we want to explain this?? The slanted feature seen in the posterior PDF is characteristic to this method, because it is a consequence of the expression $\frac{d\theta}{dt} = \omega$ discussed previously.

In summary, the forward model produces an ideal spectrogram at gridded values of θ and ω. The RBE approach, then, allows one to compute the conditional PDF of these parameters, given an observed spectrogram. Finally, the dynamic parameters are estimated to be those values which maximize that PDF.

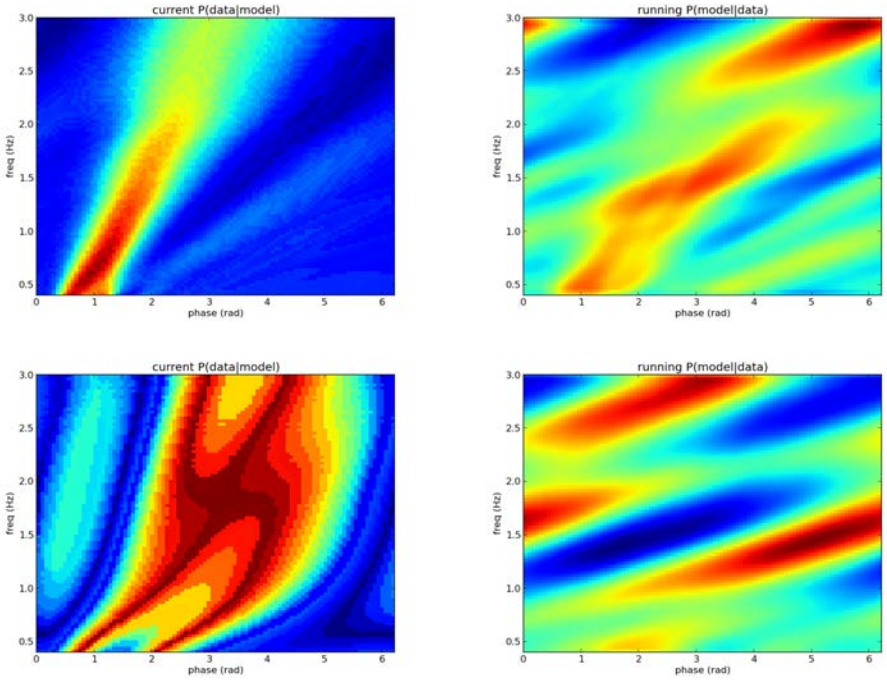

Figure 7: The likelihood (left) and the posterior PDF (right) over ω, θ, for two patients (top and bottom).

3.6 Feature Extraction

The dynamic parameters which maximize the aforementioned posterior PDF constitute a time series. Fig. 3.6 shows the time series for two dynamic parameters ω and θ as estimated according to the mode of the posterior PDF. As seen, the initial estimates change rapidly; after a few cardiac cycles the θ paremeter settles on a cyclic pattern, while the ω parameter converges onto a fixed value.

Armed with estimates of the dynamic parameters, one can generate a variety of useful quantities, such as a spectrogram, an envelope, mean flow, and even pulsutility index. An example of a predicted spectrogram is shown in Figure 3.6, where it is compared with the corresponding observed spectrogram. Evidently, the fitted spectrogram closely matches the observed

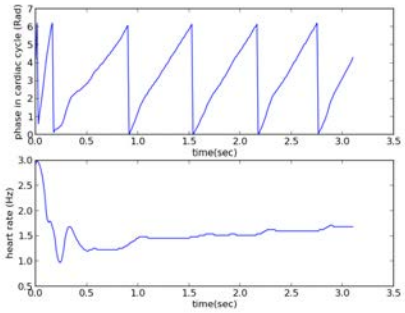

Figure 8: The output of the RBF.

spectrogram in multiple ways, For example, ?? compare the two figs - diastolic notch - body of the spectrogram - etc. including the aliasing, etc. ??

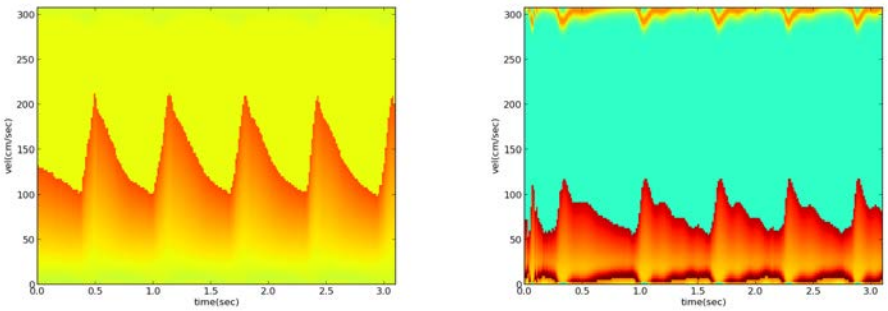

Figure 9: An example of an observed (left) and a predicted (right) spectrogram.

A pulsutility index can be constructed as follows: The pulsitility is defined [16] over a cardiac cycle as the difference between the systolic and diastolic flow velocity, divided by the mean flow velocity, where systolic and diastolic are synonomus with the maximum and minimum of flow velocity. The ω which maximizes the posterior PDF corresponds to a cardiac cycle over which the pulsitility may be computed, thus producing a time series of instantaneous pulsitility. Similarly any qunatity that may be derived from the

forward model may be presented as a time series corresponding to the most likely dynamic parameters.

4 Results

This section applies the above methodology to several patients, and diagnoses the spectrograms in terms of the more fundamental quantities such as flow fields, etc.

We should agree on how to interpret all of these results. So, for now, I'll say nothing??

I will also attempt to produce some figures that compare the predicted and observed spectrogram in a more quantitative fashion. This comparison turns out to be more complicated than might seem??

Although one aim of the present work has been to generate a predicted spectrogram, the flow field solution is the more desirable (or fundamental) quantity. However, there exists a degeneracy in the solutions that potentially prevents one from obtaining a unique, physical solution. The degeneracy can be traced to an approximation made to assure that a time wise harmonic decomposition of the boundary conditions and solutions is appropriate ([1] [3], [5], [6]). Each frequency component is solved separately, and the final solution is their linear combination across frequencies. In general, at each frequency there exists multiple solutions (i.e. degenerate modes) of flow. Often some of the modes are dismissed on the grounds that they do not meet specific requirements of the problem at hand. Combining flow field solutions to match a one dimensional time series boundary condition is possible with a linear combination of the degenerate modes for any frequency. Often in the liturature an appeal to experiment is made to resolve the true flow field [17]. In this work (following [1]) there are only two modes present, and the degeneracy is manifested in the relative phase and amplitude between the two modes, at each frequency. An estimate of this relative phase is obtained by assuming that it is constant across all freqencies. As such, the spectrogram provides sufficient information to resolve the ambiguity (because it is dependent on the entire velocity field), thus providing a unique flow field solution.

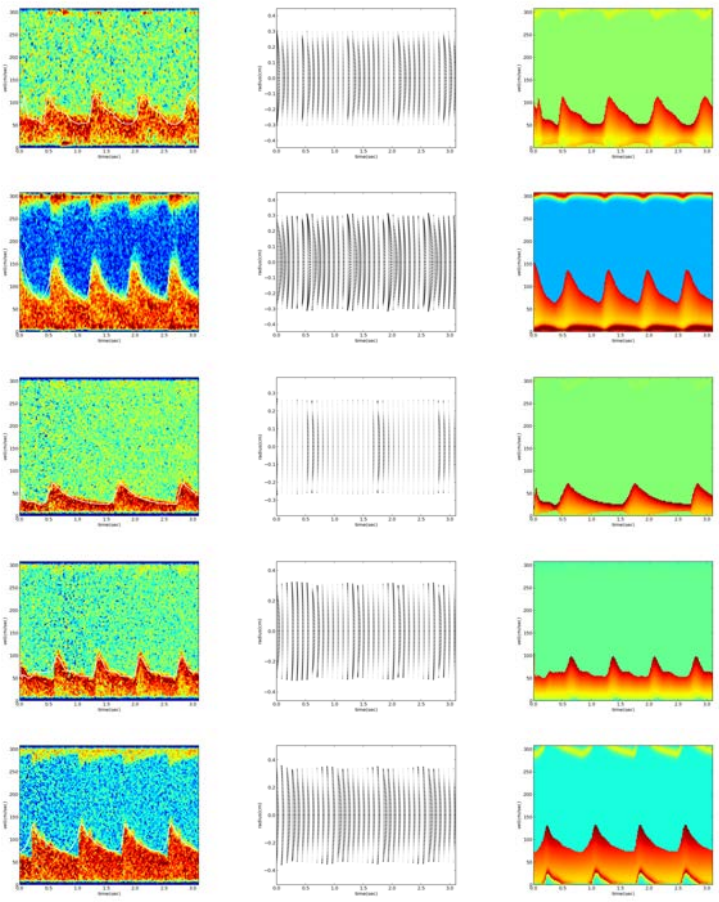

Figure 10: Observed spectrogram (left), flow field (middle), and predicted spectrogram (right) for multiple patients.

In order to address the sensitivity of the above results with respect to the choice of the fixed parameters, 100 different values of all of the fixed parameters were examined, and the root-mean-squared (RMS) error between the predicted and observed spectrogram was computed. 4 shows three of the settings which produced relatively low values of the RMS error. The columns have been positioned in increasing order of RMS error from left to right. Need to talk about these??

Overlaid in the top row is the maximum value of predicted spectrogram

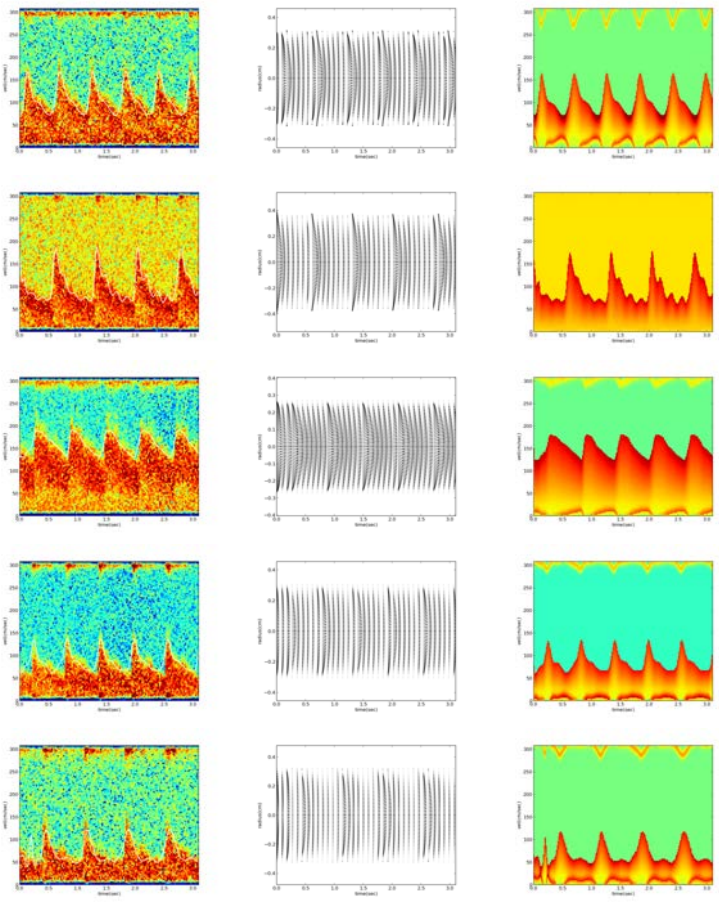

(i.e., the envelope) in white. It can be seen that there are small differences in the three envelopes. Indeed, the envelope in the middle panel appears to be more consistent with the underlying observed spectrogram. This highlights the fact that the producing spectrograms which best model the observed spectrogram may not lead to better envelopes. The next section discusses an alternative approach if the production of an envelope (and not the spectrogram) is the ultimate goal.

As discussed previously, a compairson of the predicted and observed spectrograms can aid in assessing the quality of a flow field, even though one cannot directly observe a flow field. For example, as seen in the right-most column of Fig. 4, the disagreement between the predicted and observed

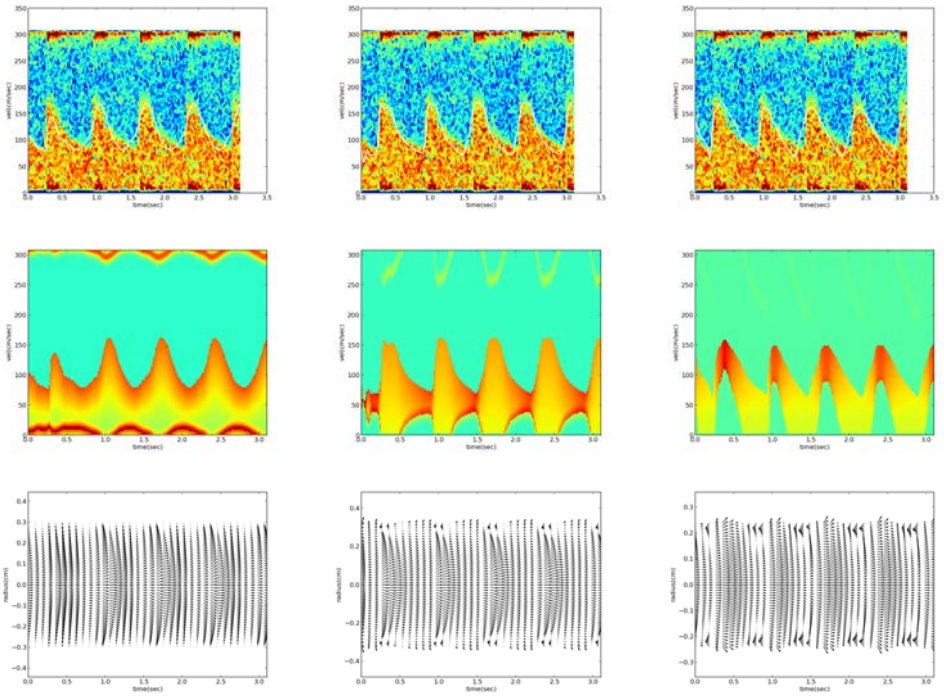

Figure 11: Observed spectrogram (top row), predicted spectrogram (middle row), and flow field (bottom row) for one patient, but with three different settings for the fixed parameters.

spectrograms implies that the flow field (shown in bottom row) is unrealistic. More ??

5 Conclusion and Discussion

A methodology has been proposed for modeling spectrograms. The approach involves a combination of physiologically-based models and statistical models. Each component of the approach involves parameters which are estimated from observed spectrograms, for a given patient. With the parameters fitted to the data from each patient, the approach produces a predicted spectrogram, which can then be used for generating summary measures such

as envelopes.

Spectrograms are useful in assessing autoregulation, i.e., the response of smooth muscle to the CO2 concentration in blood. Here, the Young's modulus, Poisson's ratio, and the rest diameter for the middle cerebral artery, are parameters which model the smooth muscle. Given that the proposed method estimates these parameters, it can therefore be considered a quantification of autoregulation.

In the illustration here, the mode of the PDF (e.g., Figure ??) was used to generate a predicted spectrogram. At each point in time, a maximum flow velocity can be obtained from that spectrogram, and the resulting time series is called an envelope. Given the probabilistic nature of the proposed methodology, one can can additionally produce a PDF of the envelope. Such a PDF can generate not only a single time series, but it can also provide a measure of uncertainty of the envelope. This can be done as follows: each value of ω and θ corresponds to a maximum flow velocity (produced by the forward model). Given a PDF of ω and θ, one can then compute a PDF for maximum flow velocity. In this way, attention is drwan away from the specific values of ω and θ which maximize their PDF, and therefore, one can compute a PDF for any quantity produced by the forward model, e.g., total flow, or pulsitility index.

Clinically, an observed spectrogram is not taken at face value, and is subjected to an internal "mental model" that exists only in a clinician's mind. The model developed here is a quantitification of that mental model. As such, an agreement between the observed and the predicted spectrogram provides the clinician an endoresment of the model and its parameter values. For example, in cases of anticipated vasospasm the mental model allows a clinician to infer changes in the radius of artery, max velocity, and total flow volume, all from the observed spectrogram. The predicted spectrogram produced by the proposed approach is implicitly based on these parameters and their values, and so is more reliable than one produced by a purely statistical model. Any uncertainty inherent in the PDF over the parameters is then due to model itself.

Another novel feature of the work here is the articulation of a closed-form relationship between a general two or three dimensional flow field and an ideal spectrogram, namely Equation 7. The utility of this expression is that

it allows one to compute a spectrogram from **any** flow field, regardless of how it is generated?? Pierre?? For example, what?? How can we make this paragraph longer??

Here the fixed parameters have not been optimized to fit the data. Instead a PDF is produced only for the dynamic parameters, using the measurement model and recursive bayesian filter approach. The outer loop showin in Figure ?? is a conceptual representation of the desire to estimate and optimize the fixed parameters. Iterating through the outerloop is a computationally intensive task. Specifically, for a single patient, one iteration requires about 1 minute of computation on a single-CPU machine. Assuming each of the parameters is sampled 10 times, a model of the type proposed (i.e., with about 20 parameters) will then require 10^{20} minutes, and is therefore entirely unfeasible.

In this paper, for the purpose of demonstrating the approach, the outer loop was not iterated a significant number of times. In applying the approach to a single patient, it was feasible to examine hundreds of iterations. But in applying it to all of the 97 patients in the data set, only tens of outer iterations were performed. A general solution to this problem would be to optimize each component of the model independently. For example, for the Circulatory System Calculation, the spectrogram could be preprocessed with and an envelope detection method to produce a time series of maximum flow along with an uncertainty about that time series. As this component is posed as a system of first order differential equations in terms fixed and dynamic paramteters, it is natural to employ a Kalman filter. In this alternative approach where the components are independently optimized, the computational requirements would be significantly lower, i.e., of the order of 10×20 minutes as compared to 10^{20} minutes noted above.

The modular nature of the proposed method allows for customized predictions. For example, in a multi-sensor situation where two spectrograms are produced for the same focal location but from different directions, only the "spectrogram calculation" component of the model need be changed. The circulatory system calculation, the flow field calculation, and the recursive bayesian filter comparison are unaffected. The inputs to the new components would involve one flow field from the flow field calculation and two observed spectrograms. The output would be the conditional probability of the two

observed spectrograms, given the flow field and the parameters of the new component.

Similarly the modular nature of the model allows for different flow velocity field calculations. For instance, closed form solutions to pulsitile fluid flow in an elastic tube date from the 50's in [5] and [3]. But more recent work develops analytic solutions for a curved artery [6]. As such, one can test Myers' model by simply replacin the component for flow-field calculation with Myers' solutions.

It is worth mentioning that for the sake of simplicity it has been assumed that the focus volume of the ultrasound is a simple cross section through the artery. This assumption constitutes an approximation to the fact that the ultrasound focus volume has a more complex spatial extent [9]. One manner in which the assumption can be relaxed is by introducing a weighting function in the numerator of the integrand of Equation 7 to account for the spatial focus of the transducer.

The construction of a model can also aid the task of locating the artery during the initial set-up of the transducer. Specifically, one can optimize the expected distance to the artery center in an automated fashion; and this would involve only the measurement model component. In this case the B mode and M mode search would be combined with the larger inversion problem.

The model proposed here includes tissue motion, and therefore, allows one to isolate the contribution (to the spectrogram) of tissue motion from blood flow. A consequence of this ability is that one can "explain" what is often referred to as aliasing, namely features at the top of the spectrogram which appear to reflect gross features at the bottom of the spectrogram. The motion of the tissue produces negative flow velocities, which are traditionally "wrapped around" and displayed at the top of the spectrogram. In the proposed model, these negative velocities can be isolated and therefore filtered-out, leading to physiologically consistent spectrograms. Figure ?? shows an illustration of this utility. The middle figure qualitativiely resembles the spectrogram (left figure); and the right figure shows the spectrogram with the negative velocities filtered out. It is important to emphasize that this filtering is physiologically based.

References

[1] Pijush K Kundu Ira M Cohen
Fluid Mechanics fourth edition
2008

[2] Taous-Meriem Laleg, , Emmanuelle Crpeau , Michel Sorine
Separation of arterial pressure into a nonlinear superposition of solitary waves and a windkessel flow
Biomedical Signal Processing and Control
Volume 2, Issue 3, July 2007, Pages 163170

[3] J.R. Womersley
Oscillatory motion of a viscous liquid in a thin walled elastic tube. I. The linear approximation for long waves.
Philosophical Magazine
1955b
46:199-221

[4] Sunghan Kim, Mateo Aboy, James McNames
Pulse pressure variation tracking using sequential Monte Carlo methods
Biomedical Signal Processing and Control
8 (2013)
333-340

[5] G.W. Morgan, J.P. Kiely
Wave Propagation in a viscous liquid contained in a flexible tube
The Journal of the Acoustical Society of America
1954
26(3):323-328

[6] Lance Jonathan Myers and Wayne Logan Capper
Analytical Solution for Pulsatile Axial Flow Velocity Waveforms in Curved Elastic Tubes
IEEE TRANSACTIONS ON BIOMEDICAL ENGINEERING
, VOL. 48, NO. 8, AUGUST 2001
864-873

[7] Mahmoud El-Gohary, Lars Holmstrom, Jessie Huisinga, Edward King, James McNames, Fay Horak

Upper limb joint angle tracking with inertial sensors.
3rd Annual International Conference of the IEEE EMBS Boston, Massachusetts USA
August 30 - September 3, 2011

[8] Technical Documentation of Nodestar
LAWRENCE D. STONE
THOMAS L. CORWIN
Metron, Inc.
Reston, VA
JAMES B. HOFMANN
AdvancedInformation Technology Branch
Information Technology Division
December 11, 1995

[9] Some Aspects of the relationship Between Instantaneous Volumetric Blood Flow and Continuous Wave Doppler Ultrasound Recordings - I
David H. Evans
Ulrasound in Medicine and Biology
volume 8 number 6
pages 605-609
first recieved 17 July 1980
final form 24 March 1982

[10] Estimation of Blood Velocities Using Ultrasound: A Signal Processing Approach
Jrgen Arendt Jensen
published March 29, 1996
need to get a hold of this and double check what it actually contains
look for further references again.

[11] Doppler ultrasound: physics, instrumentation, and signal processing
David H. Evans, W.N. McDicken
Wiley, Mar 27, 1989
also need to look through evan's book doppler ultrasound
It may well contain a closed form expression for the measurement model that's not in the journal articles.

[12] Fernando KL, Mathews VJ, Clark EB.
A mathematical basis for the application of the modified geometric

method for maximum frequency estimation.
IEEE Trans. Biomedical Engineering
2004; 51:2085-2088.

[13] A Double-Gaussian, Percentile-based Method for Estimating Maximum Blood Flow Velocity
Caren Marzban, Ph.D. , Paul R. Illian, B.S. David Morison, B.S. , Pierre D. Mourad, Ph.D.

[14] Br[itish] J[ournal] Obstet Gynaecol. 1998 Oct;105(10):1118-21.
Significance of a diastolic notch in the uterine artery flow velocity waveform induced by uterine embolisation in the pregnant ewe.
Ochi H, Matsubara K, Kusanagi Y, Taniguchi H, Ito M.
Source
Department of Obstetrics and Gynaecology, Ehime University School of Medicine, Shigenobu, Japan.
Abstract
OBJECTIVE:
To investigate the relation between placental embolisation and the diastolic notch in the uterine artery flow velocity waveform of pregnant ewes under general anaesthesia.
METHODS:
Seven pregnant ewes at a gestation 16 to 17 weeks were anaesthesized and microbeads of gelfoam were injected into the uterine artery; changes in the uterine circulation were assessed by Doppler velocimetry.
RESULTS:
Gelfoam embolisation reduced uterine blood flow in a dose-dependent manner, from a mean (95%, CI) of 568 mL/min (495-641) to 159 mL/min (131-187) after the injection of 30 mg of gelfoam, and increased the uterine vascular resistance from 135 mmHg x min x L(-1)(103-167) to 498 mmHg x min x L(-1) (422-574). A diastolic notch in uterine artery flow velocity waveform was observed after 20 mg to 25 mg of gelfoam in two ewes and after injection of 30 mg of gelfoam in all seven animals. Injection of 30 mg of gelfoam increased the pulsatility index to 2.4 (1.9-2.9) from 0.6 (0.5-0.7). The mean uterine vascular resistance at the time of the appearance of a diastolic notch was 414 mmHg x min x L(-1)(377-451).
CONCLUSION:
These findings suggest that an elevated pulsatility index and the pres-

ence of a diastolic notch in the uterine artery flow velocity waveform are indicators of increased uterine vascular resistance and impaired uterine circulation.

[15] Blood flow throught arteries in a pathological state: A theoretical study
J.C. Mirsa, G.C. Shit
International journal of Engineering Science
December 13, 2005

[16] Arterial assessment by Doppler shift ultrasound
Gosling and King 1974
R.G. Gosling, D.H. King
Proc R Soc Med, 67 (1974), pp. 447449

[17] An experimental determination of the propagation of fluid oscillations in a tube with visco-elastic wall
Phys. Med Biol.
4, 63, 1959